

Development of Kirkwood-Buff derived forcefield for phospholipids

by

Sandun Sudantha Gajaweera

B.S., Institute of Chemistry Ceylon, 2011

---

A THESIS

submitted in partial fulfillment of the  
requirements for the degree

Master of Science

Department of Chemistry  
College of Arts and Sciences

KANSAS STATE UNIVERSITY  
Manhattan, Kansas

2021

Approved by:

Major Professor  
Professor Paul E. Smith

# Copyright

© Sandun Gajaweera 2021.

# Abstract

Recently, we have developed an improved force field for the simulation of peptides and proteins. To develop accurate models for lipids, we present force field parameters for the study of 8 glycerophospholipids in water. Previous work on the forcefield includes force field parameters for the polar groups of lipids (head groups, glycerol, ester functionalities) to reproduce the experimental Kirkwood-Buff (KB) integrals for small molecule analogs and their mixtures with water. Reproducing the KB integrals is not possible for the hydrocarbon tails of lipids. Consequently, using a more traditional approach to ensure that a variety of typical properties of lipid membranes were reasonably reproduced. The electron density profiles, the area, and volume per lipid, the lipid lateral diffusion rates, and the hydrocarbon chain order parameters were investigated and compared with experimental data where available.

# Table of Contents

List of Figures . . . . .	vi
List of Tables . . . . .	ix
Acknowledgements . . . . .	x
Dedication . . . . .	xi
1 Introduction . . . . .	1
1.1 Molecular Dynamics Simulations . . . . .	1
1.2 Force Fields . . . . .	4
1.3 Lipid Membranes and Bilayers . . . . .	7
1.3.1 Lipid Shape . . . . .	11
1.3.2 Lipid Types . . . . .	11
1.3.3 Lipid Phase . . . . .	13
1.3.4 Experimental Observations of Lipid Bilayers . . . . .	15
1.3.5 Membrane Structural Analysis . . . . .	16
1.3.6 A Kirkwood-Buff Derived Force Field for Glycerophospholipids . . . . .	21
1.3.7 Kirkwood-Buff Derived Force Field for Esters . . . . .	22
1.3.8 Kirkwood-Buff Derived Force Field for Phosphate . . . . .	23
1.3.9 Kirkwood-Buff Derived Force Field for Polyols . . . . .	23
2 Single Lipid Simulations . . . . .	25
2.1 Introduction . . . . .	25
2.2 Parameter Development . . . . .	27

2.3	Molecular Dynamics Simulations . . . . .	28
2.4	Results and Discussion . . . . .	29
2.5	Conclusion . . . . .	33
3	Pure Phospholipid bilayers Simulations . . . . .	35
3.1	Introduction . . . . .	35
3.2	Methods . . . . .	36
3.2.1	Simulation System . . . . .	36
3.2.2	Simulation Parameters . . . . .	37
3.3	Results . . . . .	37
3.3.1	Area per Lipid( $A_L$ ) . . . . .	37
3.3.2	Volume per Lipid( $V_L$ ) . . . . .	38
3.3.3	Electron Density Profile(EDP) . . . . .	38
3.3.4	Deuterium Order Parameters( $S_{CD}$ ) . . . . .	41
3.3.5	Diffusion Coefficient . . . . .	41
3.4	Discussion . . . . .	43
3.5	Conclusion . . . . .	46
	Bibliography . . . . .	47

# List of Figures

1.1	A Schematic diagram of the steps in a MD simulation. Figure adapted from ref. 1;2. . . . .	4
1.2	A pictorial description of intra- and inter-molecular interaction energies and corresponding mathematical representation of energy terms . . . . .	5
1.3	Shapes of lipids and the type of lipid corresponding to its unique shape. Figure adapted from ref. 3. . . . .	9
1.4	“Representation of a characteristic glycerophospholipid, the head group substituents and the linkage between glycerol and fatty chain. (B) Representation of a characteristic sphingolipid, the head group substituent, and the different types in the sphingoid base backbone. (C) Representation of a typical sterols, i.e., cholesterol. (D), (E) N-acyl chains with various length and unsaturation, and position of the double bond. The key is of the form (XX: Y, n-Z), with XX, Y, and Z the number of carbons, double bonds, and position of the first double bond from the omega end, respectively. This key describes also the two fatty acyl chains with the form (XX: Y, n-Z): (XX: Y, n-Z). C1P: ceramide-1-phosphate, Complex GSL: complex glycosphingolipids, DHS: sphingosine, Gal Ceramide: galactosylceramide, Glc Ceramide: glucosylceramide, LBPA: lysobiphosphatidic acid, LPA: lysophosphatidic acid, PC:phosphatidylcholine, PE:phosphatidylethanolamine, PG: phosphatidylglycerol, PHS: 4-hydroxy-sphinganine, PI: phosphatidylinositol, PS: phosphatidylserine, SPH: sphingosine”. Figure adapted from ref. 3. . . . .	10

1.5	Glycerophospholipids head groups. The hydroxyl group is bound to the phosphate moiety. Figure adapted from ref. 3. . . . .	13
1.6	Electron density profile of a lipid bilayer, Figure adapted from ref. 4. . . . .	17
1.7	A Comparison between a sample of a biological membrane and a lipid synthesized by an in-vivo method. Values of the deuterium order parameter w.r.t position of the segment for the lipid POPC. Figure adapted from ref. 5;6. . . . .	20
2.1	A labeled diagram for POPC lipid . . . . .	31
2.2	The PMF ( $\text{kJmol}^{-1}$ ; y-axis) of O14C13C34O35 dihedral angle (x-axis) . . . . .	32
2.3	The PMF ( $\text{kJmol}^{-1}$ ; y-axis) of dihedral angles (x-axis) consisting of atoms, C3N4C5C6 (black), C5C6O7P8 (red), C6O7P8O11 (blue), O7P8O11C12 (brown), P8O11C12C13 (violet), in (a) and O11C12C13O14 (maroon), C12C13O14C15 (green), C13O14C15O16 (cyan), O14C13C34O35 (magenta), O14C15C17C18 (indigo) in (b) . . . . .	33
2.4	The PMF ( $\text{kJmol}^{-1}$ ; y-axis) of dihedral angle (x-axis) at cis double bond in the POPC (single lipid) acyl chain. The FFs are CHARMM36(black), GROMOS (red), OPLS (green), SLIPID (blue) . . . . .	34
3.1	Total EDP of DMPC (A), DOPC (B), POPC (C), DPPC (D), DOPE (E), DOPS (F), POPE (G), POPS (H), in black line. The Density of water is included (in black line; to complement lipid EDP). All corresponding experimental curves and models (of total electron density) developed from experimental data are in black downward triangles. All corresponding experimental curves of water developed from experimental data are in a black circle. <sup>7</sup> . . . . .	39

3.2	EDP of POPC in comparison of FFs (A; experiment-black, CHARMM36-red, GROMOS54A7-green, KBFF-blue, OPLSAA-grey, SLIPID-orange) POPC 512 lipid systems in water (B;black line). The corresponding experimental curves and models (of total electron density) developed from experimental data are in black upward triangles. <sup>7</sup> . . . . .	40
3.3	Acyl chain $S_{cd}$ of POPC $sn - 1$ , $sn - 2$ (A-i, ii), POPE $sn - 1$ , $sn - 2$ (B-i, ii), POPS $sn - 1$ , $sn - 2$ (C-i, ii), compared to that of experiment. The experimental values are adopted from ref 8;9 . . . . .	42
3.4	Acyl chain $S_{cd}$ of (A-i, ii), DOPE $sn - 1$ , $sn - 2$ (B-i, ii), DOPS $sn - 1$ , $sn - 2$ (C-i, ii), compared to that of experiment. The experimental values are adopted from ref 8;9 . . . . .	43
3.5	Acyl chain $S_{cd}$ $sn - 1$ , $sn - 2$ (A, B) of POPC 512 lipid system compared to that of experimental. The upward triangle is experimental $S_{cd}$ values, the star is $S_{cd}$ values at 200 ns, the cross is $S_{cd}$ values at 400 ns, the circle is $S_{cd}$ values at 600 ns, the square is $S_{cd}$ values at 800 ns, the diamond is $S_{cd}$ values at 1000 ns . . . . .	44

# List of Tables

1.1	commonly found phospholipids and their abbreviations. (Table adapted from ref. 3;8) . . . . .	12
2.1	Torsion angles parameters used for the glycerol backbone. Dihedral angles were defined according to Figure 2.1, where the phase shift $\delta$ is taken to be $-60$ and $+60$ for all angles . . . . .	28
2.2	The gauche and trans percentages of the glycerol backbone POPC single lipid	29
2.3	The gauche and trans percentages of the glycerol backbone POPC single lipid	30
2.4	Single lipid molecules diffusion coefficient for various lipids . . . . .	32
2.5	POPC single lipid molecule diffusion coefficient for different FFs . . . . .	32
3.1	Description of simulated systems . . . . .	36
3.2	Comparison of simulated area per lipid and experimental area per lipid . . .	37
3.3	Comparison of simulated volume per lipid and experimental volume per lipid	38
3.4	Comparison of simulated $D_{HH}$ and experimental $D_{HH}$ . . . . .	38
3.5	Diffusion coefficient(D) for lipid bilayer systems. A comparison of simulated $D(\text{cm}^2\text{S}^{-1} \times 10^{-8})$ and experimental $D(\text{cm}^2\text{S}^{-1} \times 10^{-8})$ . . . . .	41
3.6	Diffusion coefficient(D) <b>POPC</b> for Different FFs . . . . .	42

# Acknowledgments

I would like to thank my mentor Dr. Jeffrey Comer for his invaluable support, tutelage and advice which help me navigate through this difficult time in revising and submitting my Masters thesis. I'm grateful to the review committee of Dr. Beth Montelone, Dr. Amit Chakrabarti, Dr. David V. Rosowsky and Dr. Daniel A. Higgins for their patience and objective perspective. I would like to extend my gratitude to students Ombudsperson Kimathi Choma for his support. I would like to thank Dr. Elizabeth Ploetz for taking the time out of her busy schedule to point out some much needed revisions that added value to my thesis. I'm sincerely grateful to Dr. Samntha Weerasinghe for guiding me through my graduate studies in Sri Lanka and introducing me to Dr. Paul E Smith. I extend my gratitude to Dr. Paul E Smith for taking on the task as external examiner to assess my previous graduate dissertation work done in Sri Lanka, recruiting me for the Chemistry PhD program at Kansas State University as a PhD student to work in his lab. Furthermore I would like to thank my Master's supervisory committee. I would like to thank my lab mates Nilusha, Nawavi for their support. Finally, I'm grateful to my family for all the support they have given me while preparing this dissertation.

# Dedication

I dedicate my dissertation to my loving wife Jeeva and my three puppies Misha, Lars and Flounder for their endless love and support.

# Chapter 1

## Introduction

### 1.1 Molecular Dynamics Simulations

Molecular simulations are a powerful set of tools which can provide atomic level detail of various types of biological systems that may not be so easily obtained by using experimental methods.<sup>10</sup> The two main methods that use classical physics are called molecular dynamics (MD) and Monte- Carlo (MC) calculations. Thermodynamic properties, such as chemical potentials, heat capacities, partial molar volumes, and compressibility, can be obtained from both MD and MC simulations, while kinetic properties, such as diffusion coefficients, viscosity, relaxation times, and permeability, can be calculated from MD simulations but are typically unavailable in MC calculations since the MC trajectory does not represent true time evolution of the system.<sup>11</sup> The study discussed in this thesis is based on MD simulations

The main purpose of using MD and MC simulations, is to relate microscopic properties of the system to macroscopic properties, using statistical thermodynamics.<sup>12</sup> Molecular simulations can provide atomic level detail of complex physical phenomena that cannot be described solely dependent on experimental studies.<sup>13</sup> Thus, simulations can be considered as a bridge between experiment and theory.

Certain experiments require extreme conditions such as high pressure, high temperatures and radioactive environments which could not only be expensive but very hazardous, ren-

dering them inaccessible to most researchers under typical laboratory conditions. However, simulations can offer a safe alternative to this type of experiments at a fraction of the price.<sup>14</sup>

Quantum mechanical models of molecules give an accurate description as to how well the molecules samples phase space.<sup>15</sup> However, quantum mechanical simulations treat molecules at a subatomic level incorporating the behavior of electrons within an atom.<sup>16</sup> These types of calculations are very expensive to carry out even in modern day computers. On the other hand, MD simulations treat atoms using the Born-Oppenheimer approximation, which allows the use of classical mechanics to describe the movement of atoms.<sup>17</sup> Therefore, larger more complex systems such as peptides and proteins with around  $1 \times 10^5$  atoms or more can be simulated in a matter of hours.<sup>18</sup>

In MD simulations, Newtons equations of motion are approximated over a finite time to describe the movement of each atom in the system. The atoms in a molecule are represented as soft spheres and bonds are represented as springs that oscillate in some form of simple harmonic motion.<sup>19</sup> The objective of using classical mechanics is to determine the forces acting on each atom of a molecule which transcends to the forces acting on the molecule, and consequently the forces acting on the system. The change in forces within the system is then used to determine the change in properties of the said system.<sup>1</sup> The first derivative of potential energy ( $P.E = U$ ) is used to determine the force acting on a molecule as shown in equations 1.1 and 1.2.

$$m_i \ddot{r}_i = f_i \tag{1.1}$$

$$f_i = -\frac{\partial U}{\partial r_i} \tag{1.2}$$

According to 1.1 and 1.2, the force exerted on  $i^{th}$  particle with mass  $m_i$  and acceleration  $\ddot{r}_i$  is  $f_i$ . Here the second derivative of  $\ddot{r}_i$  w.r.t time gives the acceleration of the particle denoted as  $\ddot{r}_i$ . The force calculation is vital in determining the next state of the system. The equations of motion are solved using numerical analysis. The differential equations related to motion are approximated using finite difference methods.<sup>16;20</sup> The goal is to use the ve-

locity and position of the system from the previous state and in the current state to predict the new velocities and position and forces in a finite time step. The Verlet algorithm is a widely used algorithm in MD simulations to predict the next step in the system by solving equations of motion.<sup>20;21</sup> All algorithms assume the dynamic properties and positions can be approximated using Taylor series expansion. As described in equations 1.3 and 1.4 the current position  $\vec{r}(t)$  and previous position  $\vec{r}(t-\delta t)$  is used to predict the next position  $\vec{r}(t+\delta t)$  of molecules in the system.

$$\vec{r}(t + \delta t) = \vec{r}(t) + \delta t \vec{v}(t) + \frac{1}{2} \delta t^2 \vec{a}(t) + \dots \quad (1.3)$$

$$\vec{r}(t - \delta t) = \vec{r}(t) - \delta t \vec{v}(t) + \frac{1}{2} \delta t^2 \vec{a}(t) - \dots \quad (1.4)$$

The terms  $\vec{r}(t)$ ,  $\vec{v}(t)$ ,  $\vec{a}(t)$  and  $\delta t$ , represents the current position, velocity, acceleration, and finite time step, respectively. If one is to add equation 1.3 and 1.4 the resulting equation 1.5 is independent of velocity

$$\vec{r}(t + \delta t) = 2\vec{r}(t) - \vec{r}(t - \delta t) + \delta t^2 \vec{a}(t) \quad (1.5)$$

Although the velocity is not required to determine the next position  $\vec{r}(t + \delta t)$ , it is necessary for the calculation of kinetic energy (K.E). Hence velocity is calculated using equation 1.6.

$$\vec{v}(t) = \frac{\vec{r}(t + \delta t) - \vec{r}(t - \delta t)}{2\delta t} \quad (1.6)$$

The size of the time step depends on the system that is simulated. The main steps in a MD simulation can be simplified as shown in Figure 1.1 MD simulations can be used to study both equilibrium and non-equilibrium systems. In an equilibrium system there is no net transport of mass, momentum, and heat. However, it becomes very difficult to establish a link between dynamic properties at the microscopic state to non-equilibrium macroscopic

state if the system is far from the equilibrium.<sup>22</sup> These type of perturbations from equilibrium can be studied using non-equilibrium molecular dynamics simulations (NEMD).

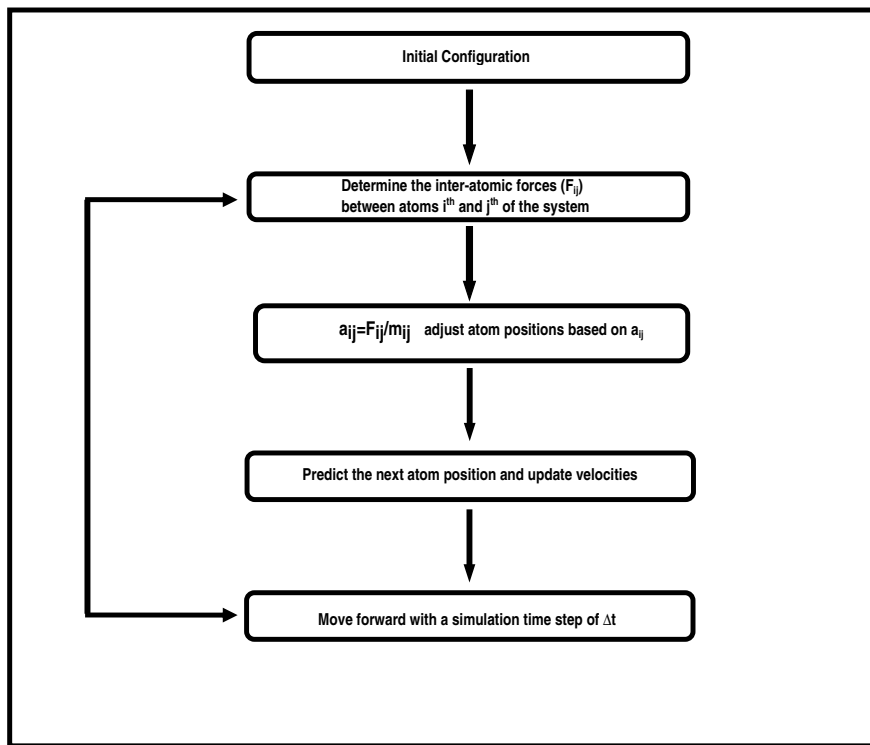


**Figure 1.1:** A Schematic diagram of the steps in a MD simulation. Figure adapted from ref. 1;2.

This dissertation is solely based on equilibrium MD simulations.

## 1.2 Force Fields

In MD simulations the potential energy of a system is calculated using a force field. In a force field electron motion is ignored (Born-Oppenheimer approximation) and the energy of the system is a function of the nuclear position. Therefore, molecular simulations perform calculations on systems with  $1 \times 10^3$  to  $1 \times 10^6$  atoms. In certain cases force fields provide accuracy that is given by the highest level of quantum chemical calculations at a fraction of computational cost. The force field can be interpreted using four components which represent inter and intra-molecular forces in the system.<sup>11</sup>

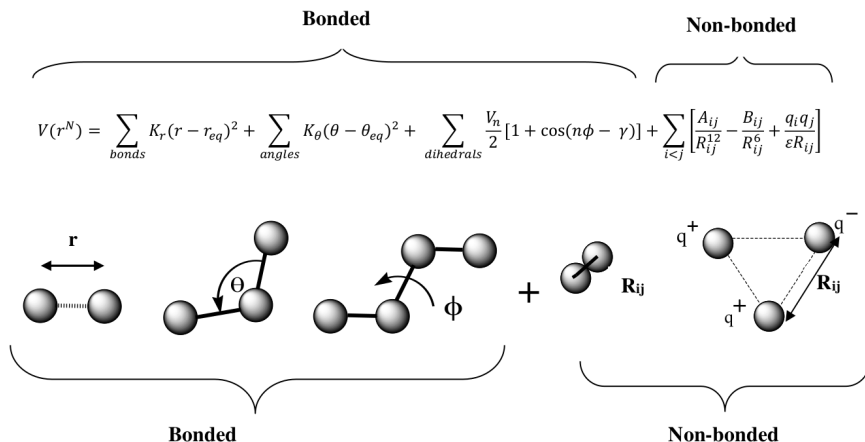


**Figure 1.2:** A pictorial description of intra- and inter-molecular interaction energies and corresponding mathematical representation of energy terms

The interaction energy of the system is modeled using the equation depicted in Figure 1.2. The force-field equation treats the potential energy of the system as two separate parts: bonded and non-bonded interaction energies. The bonded interaction (intra-molecular forces) terms restrict deviations in bond length, bond angles and dihedral angles from their equilibrium values. The non-bonded interactions (inter-molecular forces) are calculated between pairs of atoms (usually denoted as  $i$  and  $j$ ) that are in different molecules or within the same molecule but separated by at least three bonds. These non-bonded interactions are described by van der Waals forces and electrostatic interactions. The energy contributions by van der Waals forces are modeled using Lennard-Jones potential function while electrostatic interactions are modeled using Coulomb's law.<sup>11</sup> A thorough description of each component in Figure 1.2 is necessary to fully appreciate the context of this thesis.

Since the PE of the system is a function of atomic position for  $N$  atoms in the system can be represented using Cartesian coordinates ( $\mathbf{r}^N$ ). The ( $\mathbf{r}^N$ ) coordinate set can then be used to obtain internal coordinates for bond lengths ( $b$ ), bond angles ( $\theta$ ), proper and improper dihedral angles ( $\phi$ ) and inter-atomic distances ( $r_{ij}$ ) for any pair of atoms  $i$  and  $j$  as described above. The bond stretching, angle bending, [dihedral angles](#) are described using a simple harmonic energetic functions. These functions are described by stretching, bending, proper dihedral and improper dihedral respectively. As shown in Figure 1.2 equilibrium positions for

bond stretching is  $b_0$ , and the respective force constant is  $k_b$ . Similarly equilibrium positions for angle bending, and improper dihedral rotation are represented by  $\theta_0$  and  $\xi_0$  while their force constants are represented by  $k_\theta$  and  $k_\xi$  respectively. As shown by Figure 1.2 proper dihedrals are calculated between atom pair  $i$  and  $j$  such that they are separated by 3 bonds, with a force constant  $k_\phi$ , periodicity  $n$  and phase difference  $\phi_s$ . As explained earlier non-bonded interactions are calculated between atoms in different molecules or atoms within the same molecule. In the case of the same molecule the interaction between atom pair  $i$  and  $j$  should be calculated when the atom pair is  $n \geq 4$  bonds apart. The partial atomic charges ( $q^i, q^j$ ) are used to calculate electrostatic interactions (Coulombic forces).<sup>23</sup>

As described in Figure 1.2 the van der Waals interaction between atoms is determined from a Lennard-Jones (12 - 6) potential (LJ potential). As depicted by Figure 1.2 the parameters,  $\epsilon_{ij}$  represents well depth and  $\sigma_{ij}$  is the radius where the potential energy reaches zero ( $\lim_{r_{ij} \rightarrow 0} f(V_{r_{ij}})$ ). The attractive London dispersion forces, described by  $(\frac{1}{r_{ij}})^6$  term is a result of instantaneous induced dipole-induced dipole interaction. The repulsive force between two atoms, is a result from the repulsion between overlapping electron clouds of the said atoms, explained by the Pauli exclusion principle and is represented by  $((\frac{1}{r_{ij}})^{12})$ .

The parameters  $\epsilon_{ij}$  and  $\sigma_{ij}$  are determined for individual atom types, since it is impractical to determine  $\epsilon_{ij}$  and  $\sigma_{ij}$  for every possible atom pair. The Lorentz-Berthelot combination rules are typically used to calculate  $\epsilon_{ij}$  and  $\sigma_{ij}$ . The well depth,  $\epsilon_{ij}$ , is calculated via geometric mean and radius,  $\sigma_{ij}$ , is calculated via arithmetic mean.<sup>23</sup>

The electrostatic interactions depend on the partial atomic charges  $q_i$  and  $q_j$  of atom pair  $i$  and  $j$ , at a distance  $r_{ij}$  as shown in Figure 1.2. Although partial atomic charges are obtained from QM calculations in gas phase, these charges fail to include polarization effects in condensed phase. Thus, to account for the failure, partial atomic charges are optimized to overestimate the dipole moments of small molecules.<sup>24</sup> The polarization is explicitly treated using induced dipole models or fluctuation charge models. A more attractive alternative to explicitly treating polarization is optimizing partial atomic charges to reproduce Kirkwood-Buff (KB) integrals. This method implicitly accommodates polarization, because the parameterization is implemented to reproduce properties in liquid mixtures.<sup>25</sup> The force

fields (FF) that are mainly available for simulations of bio-molecules are categorized as all atom (AA), united atom (UA) and coarse grained (CG).<sup>26;27</sup> The AA FFs treat all the atoms in the system explicitly, while in UA FFs explicitly treat the heavy atoms and the polar hydrogen atoms. Thus, in the UA approach remaining hydrogen atoms are attached to carbon atoms. In the CG approach a selected set of atoms are treated as a single particle. The use of each approach depends on which method better suits the purpose of sampling more phase space and efficiency of simulations of macro-molecules, thereby extending the time scales possible degrees of freedom.

Most widely used AA FFs are AMBER, CHARMM, whereas a popular UA FF is GRO-MOS while a well-liked CG FF is Martini.<sup>26-28</sup> The afore mentioned systems used to optimize FF parameter solvent can be represented explicit or implicit. In the case of implicit solvent, a distance dependent dielectric constant compensates for the solvent-solute and solvent-solvent interactions. However, in the explicit case solvent medium is represented solute molecules with a dielectric constant of 1.<sup>29</sup> While considering other FFs equilibration and sampling issues is a problem of all types of simulation studies. In the case of pure lipid bilayers, the accepted standard is several hundred *ns* simulations, which will be sufficient time for equilibration and the collection averages.<sup>30</sup>

### 1.3 Lipid Membranes and Bilayers

The cell is separated as inner and outer compartments by membranes. The main constituent of membranes are lipids arranged in bilayers<sup>31</sup>, whereas the other constituents mostly include proteins<sup>?</sup>, cholesterol<sup>?</sup>, and other types of carbohydrates.<sup>32</sup> Although the lipid bilayers can be very dynamic, they are highly regulated. The chemical structure and the composition of lipids differ for various membranes (e.g.: tissues, cells, organelles). At times composition may change from one leaflet in the bilayer to another and to different sub domains within the same bilayer. The variation in lipid composition effects the fluidity, curvature, lipid phase among other important physical properties of membranes. Biophysical techniques such as high-resolution spectroscopy, solid-state nuclear magnetic resonance (NMR), X-ray

diffraction and atomic-force microscopy (AFM) are primarily used to study the physical properties of membranes.<sup>32</sup>

The spatiotemporal dynamics of lipids and membrane proteins have been extensively studied using experimental methods such as single cell particle tracking (SPT), fluorescence correlation spectroscopy (FCS).<sup>33-35</sup> These studies have revealed the membrane to be heterogeneous ( $> 10$  nm length scale) and have similar heterogeneous dynamics. The same nanoscale heterogeneity is observed in model systems used in experiments. The heterogeneous dynamics of these systems (heterogeneous) seems to occur below the nanometer length scale and nanosecond time scale. At smaller scales MD simulations is an ideal tool to rationalize the membrane heterogeneity and related dynamics at atomic level detail.<sup>35</sup>

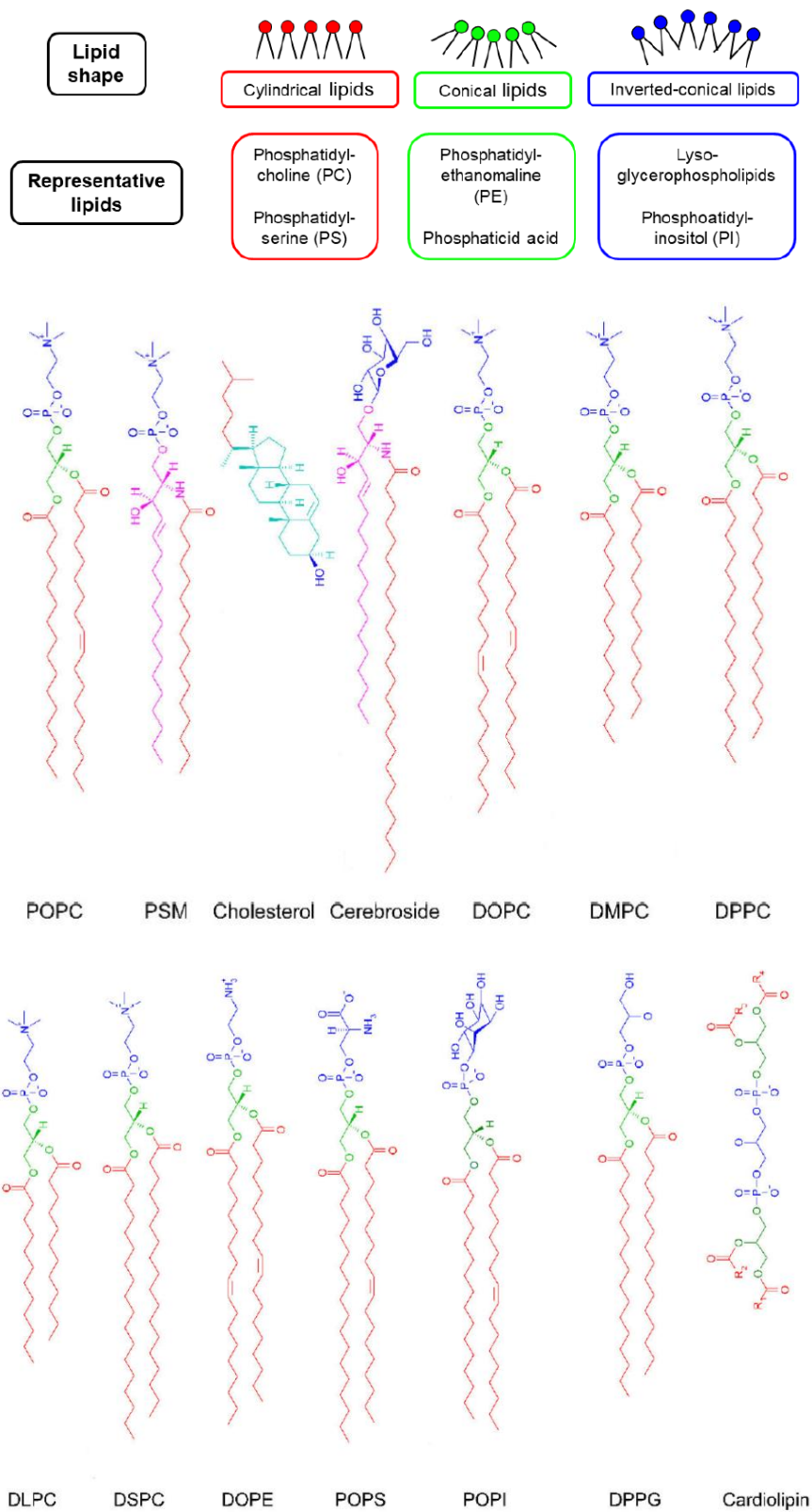


**Figure 1.3:** Shapes of lipids and the type of lipid corresponding to its unique shape. Figure adapted from ref. 3.

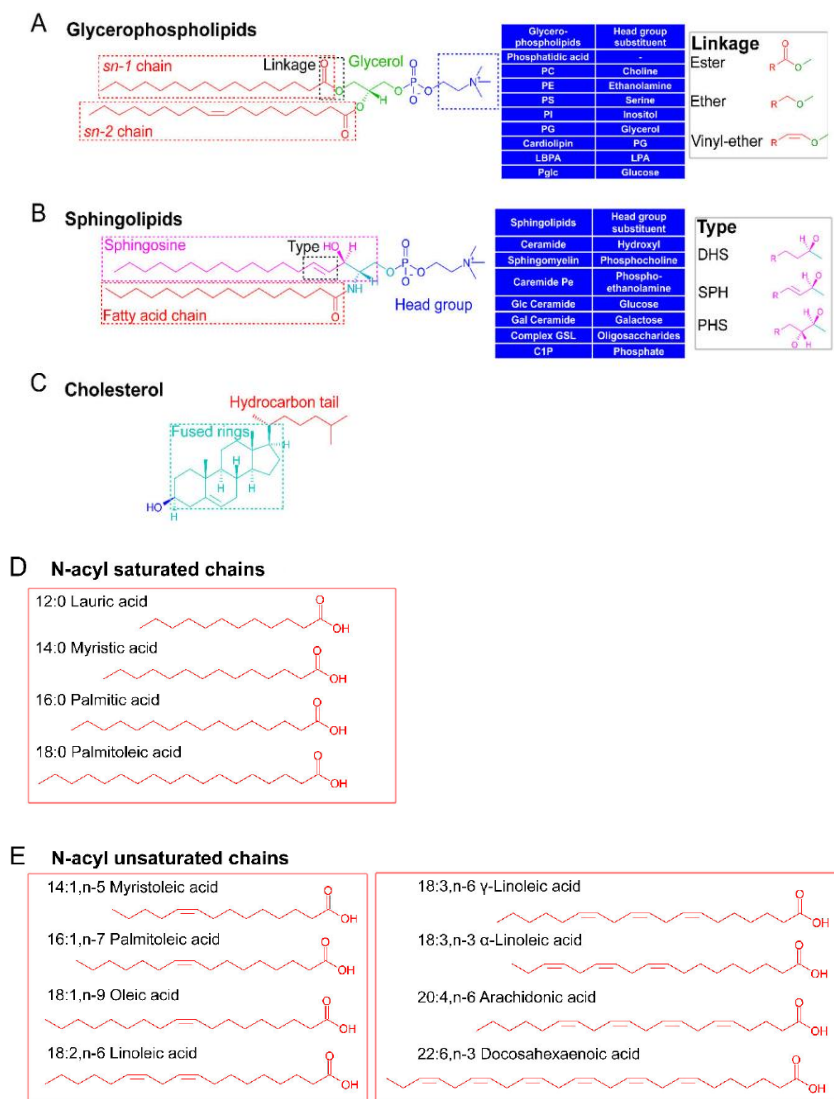


**Figure 1.4:** “Representation of a characteristic glycerophospholipid, the head group substituents and the linkage between glycerol and fatty chain. (B) Representation of a characteristic sphingolipid, the head group substituent, and the different types in the sphingoid base backbone. (C) Representation of a typical sterols, i.e., cholesterol. (D), (E) N-acyl chains with various length and unsaturation, and position of the double bond. The key is of the form (XX: Y, n-Z), with XX, Y, and Z the number of carbons, double bonds, and position of the first double bond from the omega end, respectively. This key describes also the two fatty acyl chains with the form (XX: Y, n-Z): (XX: Y, n-Z). C1P: ceramide-1-phosphate, Complex GSL: complex glycosphingolipids, DHS: sphingosine, Gal Ceramide: galactosylceramide, Glc Ceramide: glucosylceramide, LBPA: lysobiphosphatidic acid, LPA: lysophosphatidic acid, PC:phosphatidylcholine, PE:phosphatidylethanolamine, PG: phosphatidylglycerol, PHS: 4-hydroxy-sphinganine, PI: phosphatidylinositol, PS: phosphatidylserine, SPH: sphingosine”. Figure adapted from ref. 3.

### 1.3.1 Lipid Shape

A schematic representation of the lipids shape with their representative lipids for each shape. The shape of the lipid bilayer is affected by the size of the head group and the acyl chains.<sup>3</sup> As depicted in Figure 1.3, lipids with a cylindrical shape such as PC and PS, form flat bilayers. Conical shaped lipids, such as PE with a smaller sized head group and unsaturated acyl chains, can acquire a negative curvature as shown in Figure 1.4 (adapted from ref. 3). This type of lipids cause disruption in bilayers by embedding proteins in a bilayer and modifying proteins (using the ethanolamine group).<sup>36</sup> Lipids with large head groups and short acyl chains (e.g.: PI) form a positive curvature as depicted in Figure 1.4 (Figure adapted from ref. 3), give rise to inverted conical lipids bilayers.

### 1.3.2 Lipid Types

This category of lipids participates in forming membrane trafficking vesicles and protein regulation. In general, glycerophospholipids are the predominant lipid type in biological membranes. As described in 1.4 (Figure adapted from ref. 3), cardiolipin is a dimer of phosphatidylglycerol making it a special type of lipid compared to other glycerophospholipids. Although cardiolipin with di-unsaturated acyl chains predominate human membranes, it may vary for different organisms.<sup>37</sup>

The four main types of lipids are glycerophospholipids, sphingolipids, glycolipids, and sterols (cholesterol in mammals). The first three types constitute of a polar head group, glycerol backbone and acyl chains as three separate blocks which add up to form a lipid molecule. The acyl chain block comprises of one to two chains. In most cases the chains are different in length and are specified as *sn*-1 and *sn*-2.

The acyl chains are numbered such that the first number stands for the total number of carbon atoms in the chain, and the second number is the amount of unsaturation. Hence an eighteen C atom long saturated acyl chain will be represented as 18 : 0. In a case, where unsaturation is present, 18 : 2 denotes the 18 C atom long chain has two double bonds (which primarily stays in a *cis* conformation). Thus, the acronyms for glycerophospholipids

are a combination of the first two letters representing the acyl chains and last two letters representing the polar head group as described in Table 1.1. (Table adapted from ref. 3;8).

**Table 1.1:** *commonly found phospholipids and their abbreviations. (Table adapted from ref. 3;8)*

<b>Abbreviation</b>	<b>chemical name</b>
DOPC	1,2-dioleoyl-sn-glycero-3-phosphatidylcholine
POPC	1-palmitoyl-2-oleoyl-sn-glycero-3-phosphocholine
DPPC	1,2-dipalmitoyl-sn-glycero-3-phosphocholine
DMPC	1,2-dimyristoyl-sn-glycero-3-phosphocholine
DLPC	1,2-dilauroyl-sn-3-phosphocholine
DSPC	1,2-distearoyl-sn-3-glycero-phosphocholine
DOPE	1,2-dioleoyl-sn-glycero-phosphoethanolamine
POPS	1-palmitoyl-2-oleyl-sn-glycero-3-phospho-L-serine
POPI	1-palmitoyl-2-oleyl-sn-glycero-3-phosphoinositol
PSM	N-palmitoylsphingomyelin

Analogous to glycerophospholipids, sphingolipids vary to one another depending on the head group, acyl chain length and the sphingoid backbone. Lipid diversity is further provided by different head groups as shown in Figure 1.4 (Figure adapted from ref. 3).

There are three subclasses of glycolipids, (i) Oligosaccharide (or monosaccharide) linked to two acyl chains (glycoglycerolipids), (ii) An ether (e.g.: cerebroside) linking one or more sugar unit to a sphingosine and an acyl chain (glycosphingolipids), (iii) A phosphatidylinositol, with several sugars attached to the inositol group (glycophosphatidylinositol). Sterols are an important constituent of lipids and are made up of fused rings, a hydroxyl group, a hydrocarbon tail, as shown in Figure 1.4 (Figure adapted from ref. 3). As depicted in Figure 1.4, the sterol, hydroxyl group is oriented toward bulk water while being embedded in the bilayer polar head group. At the same time the hydrocarbon chain is oriented towards the bilayer hydrophobic region. Sterols can change the ordering of lipid bilayer acyl chains, hence dictating which phase the lipid exists.<sup>3</sup>

Glycerolipids are a group of lipids consisting of mono, di or tri substituted glycerol and no polar head group. As shown in Figure 1.5, the most studied group are the triesters of glycerols (triglycerides), known as triacylglycerol.<sup>3</sup> Triglycerides consist of three glycerols



**Figure 1.5:** *Glycerophospholipids head groups. The hydroxyl group is bound to the phosphate moiety. Figure adapted from ref. 3.*

linked to three acyl chains with varying degrees of unsaturation, (of varying number of carbons:14,16,18) by an ester moiety. Although Glycerolipids are used to store energy in humans, they are not components of lipid bilayer membranes.

### 1.3.3 Lipid Phase

The composition of a lipid bilayers determines their physical properties such as organization, phase, thickness, curvature, area per lipid and order parameter. The phase of lipid bilayers is related to its organization and fluidity.<sup>3</sup> The three major phases of lipids are:

**i** The liquid disordered phase ( $L_D$ ), better known as fluid phase or liquid crystalline phase ( $L_\alpha$ ). The  $L_\alpha$  phase is very fluid and has limited order. Lipids with short or unstaturated acyl chains are in the  $L_\alpha$  phase.<sup>3</sup>

**ii** The liquid ordered phase ( $L_O$ ) is highl highly ordered, yet retains some level of flexibility (not as fluid as ( $L_\alpha$ )). Furthermore this pahse contains considerable amount of cholestrol.<sup>3</sup>

**iii** The gel phase ( $S_O$ ), or the crystalline phase ( $L_\beta$ ), is highly ordered and has negligible fluidity. These type of lipids align to form crystals with their long acyl chains.<sup>3</sup> Through experiment Snyder et al., showed that during the phase transition from gel  $\rightarrow$  liquid crystal, phospholipids show an increase in gauche rotamers.<sup>38;39</sup> The presence of all-trans polymethylene chains is characteristic of the gel phase. In this study we are only interested in the liquid phase because all experimental studies used to parameterize and validate our simulation model is done at room temperature are mainly carried out for liquid phase

In experiment, pure phospholipid bilayers go through a phase transition from a gel phase at low temperatures to a disordered phase at high temperature. In the gel phase a lipids location is ordered on a two-dimensional lattice in the membrane plane and has ordered chains. This phase is also referred to as solid-ordered ( $S_o$ ).<sup>40</sup> At high temperatures, the position of lipids in the plane bear, a resemblance to a two-dimensional liquid and has disordered chains.<sup>41</sup>

Hence, the liquid-crystalline phase (high temperature or fluid phase) is called liquid-disordered ( $L_d$ ). Cholesterol prompt conformational ordering of the disordered fluid-phase lipid chains. Additionally, cholesterol molecules upset the lateral packing of low-temperature gel-phase bilayers. Therefore, cholesterol alters both the high-temperature fluid phase and the gel phase into a new phase, called, the liquid-ordered ( $L_o$ ).<sup>3;41</sup>

Although the liquid ordered ( $L_o$ ) phase resembles a liquid structure in the membrane plane it has ordered fatty acid chains. MD simulations of lipid bilayers at high temperatures have shown that cholesterol continuously orders the conformational degrees of freedom in the  $L_d$  phase.<sup>42</sup>

The simulations demonstrate a steady change in the properties of the system (cannot observe abrupt variations in chain order or area), which would imply a correct first-order phase transition with the cholesterol concentration. Nevertheless, it may be due to the presence of a critical point that margin the two-phase region at a temperature below the temperature of simulations.<sup>3;41</sup>

A phase transition is at a higher order and challenging to see in MD simulations, due to the limited system size as well as obstacles in monitoring higher derivatives accurately. Nevertheless, atomistic simulations cannot support a two-phase region beyond the gel-liquid crystalline phase transition.<sup>40</sup>

Simulations have shown the phase transition from the  $L_\alpha$  phase to the  $L_\beta$  phase by studying the surface area per lipid and the order of molecules acquired using radial distribution functions. MD simulations have been extensively utilized to study separate phases of lipid bilayers. However, MD simulations of phase transition are sparse compared to CG simulations.<sup>3;41</sup>

Fluid phase or liquid disordered is the most widespread phase in which the fatty acid chains are fully disordered. This phase is observed at high temperatures varying on the lipid composition (or pure lipid) of the membrane. The main qualities of the fluid phase are high lipid mobility and chain flexibility.<sup>3;41</sup> The  $L_\alpha$  phase has been extensively studied using varying experimental and computational techniques. The focus of this thesis is the  $L_\alpha$  phase of pure lipid bilayers.<sup>43</sup> As will be demonstrated in the following chapters our FF successfully reproduced the mobility and chain flexibility of the  $L_\alpha$  phase.<sup>3;7;44</sup>

### 1.3.4 Experimental Observations of Lipid Bilayers

Simulation data must be validated against experimental data because MD simulations are based on models. Hence, if the simulation gives good agreement with experimental data, it is pragmatic to place confidence in the model, and use simulations to understand the phenomena that cannot be studied by experiment. Only a few properties in a bilayer can be directly compared with simulation data. These are electron density profiles, order parameters, gauche-trans isomerization in bonds, volume per lipid, area per lipid, bilayer thickness ( $D_B$ ), bilayer electrostatic dipole potential and number of water molecules bound to a lipid molecule. The following discussion is an outline about experimental techniques used to study lipid bilayers.

The most effective methods to study lipid bilayer structure at atomic level are Neutron and X-ray diffraction. Although, the liquid crystalline phase is highly disordered a few diffraction peaks can be observed.<sup>44</sup> Therefore, diffraction data are available for DOPC and DPPC bilayers, where a proposed theory account for the large undulation fluctuations of the bilayer. The data obtained from this technique are bilayer form factors, which are then transformed to determine electron density profiles, electron density profile peak to peak distance, area per lipid, volume per lipid, Number of water molecules per lipid at full hydration, chain tilt angle, headgroup tilt angle and the bilayer repeat spacing. Another interesting technique is the  $^{13}\text{C} - H$  relaxation times at multiple positions in lipids using NMR spectroscopy.<sup>45</sup> In these experiments relaxation times are obtained at different field strengths. The time corre-

lation functions of C-H vectors can be used to compare the fast motions in experiment to that of simulations, and validate the simulation-dynamics. However, measuring order parameter of deuterated lipids using NMR is widely used. Order parameters are an accurately determined experimental property that can be compared with easily obtainable simulated order parameters. Many more techniques are used to study lipid bilayer properties, Fluorescence measurements (using fluorescent markers), black file measurements to determine permeabilities, ESR spectroscopy, IR/Raman spectroscopy to study dihedral gauche defects in lipid acyl chains and differential scanning calorimetry to study phase transitions.<sup>7</sup>

### 1.3.5 Membrane Structural Analysis

Electron density profiles can provide a description about the structure of lipid bilayers. Knowing the type of atoms in the system aids to determine positions of certain atoms and molecule using electron density distributions. In computer simulations a similar method is used to determine the structure and characterize certain properties of simulated systems.<sup>4</sup> In MD simulations histograms of electron distributions are computed for every atom. [The electron density profiles obtained from simulations, are directly compared with experimentally determined values \(from x-ray or neutron scattering\).](#)<sup>46</sup> (all equations w.r.t edp are adapted from ref. 4):

$$S(q) = \int_{-\frac{D}{2}}^{\frac{D}{2}} [\rho(z) - \rho_w] \cos(qz) dz \quad (1.7)$$

$$D_B = D - \int_{-\frac{D}{2}}^{\frac{D}{2}} [\rho_w(z)] dz \quad (1.8)$$

$$2D_C = \int_{-\frac{D}{2}}^{\frac{D}{2}} [\rho_{CH_2}(z)] dz \quad (1.9)$$

$$\rho_{CH}(z) = \rho_{CH_2}(z) + \rho_{CH_3}(z) \quad (1.10)$$

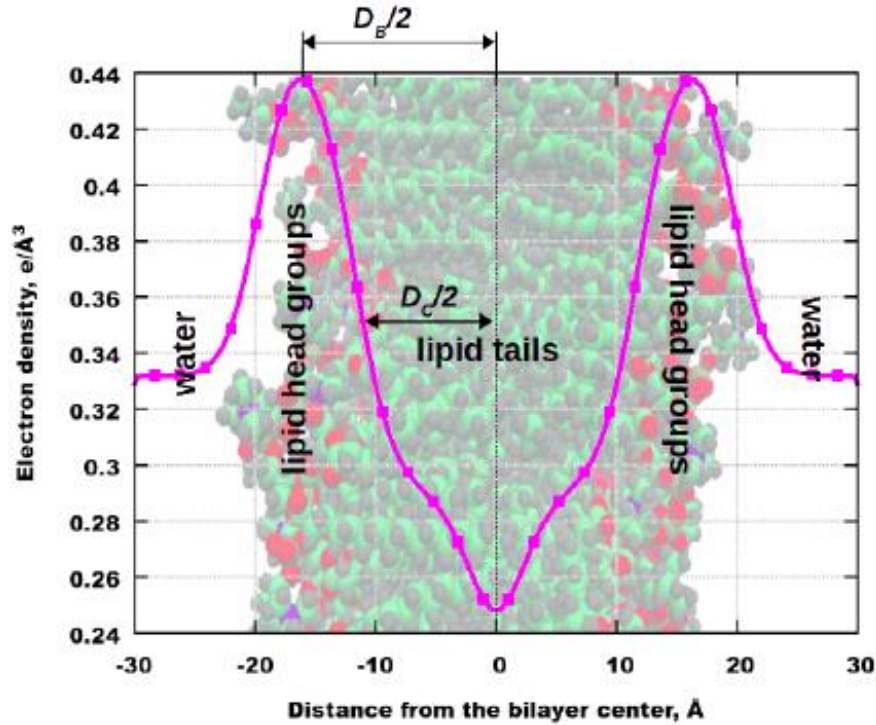


**Figure 1.6:** *Electron density profile of a lipid bilayer, Figure adapted from ref. 4.*

In equation 1.7  $\rho(z)$  stands for electron density along z-axis, which is computed from the atomic partial charges,  $\rho_w$  is the electron density of water,  $D$  denotes the size of the simulation box along z-axis which also corresponds to the D-spacing of membranes in scattering experiments. Hence with access to density properties data such as Luzatti thickness,  $D_B$

In equation  $\rho_w(z)$  denotes the probability distribution along z-direction of water. As shown in Figure 1.6 the thickness of the hydrophobic region,  $2D_C$  of the membrane can likewise be computed as shown in equation

The  $P_{CH}$  (thickness of the hydrocarbon region) is computed as described in equation, 1.10 The membrane thickness is a parameter that is highly dependent on lipid composition. For example, due to the modulatory effect of cholesterol a lipid bilayer is thicker with cholesterol compared to that of a bilayer without it. Although the definition of membrane thickness may seem intuitive, there are several modes of thickness depending on how lipid boundaries are defined.<sup>4</sup> Membrane thickness calculations include, (all equations w.r.t lipid thickness are adapted from ref. 3;4)

**i** The head group to head group distance (Head-to-Head distance  $D_{HH}$ ) of the two leaflets is the distance between the peaks of electron density profile (explained below). The value of  $D_{HH}$  can be obtained both experimentally and theoretically

**ii** By measuring the distance between the center of mass of the lipid phosphate moieties, this can be obtained only theoretically

**iii** The hydrocarbon chain thickness  $2D_C$  and half thickness  $D_C$  is deduced using the partial head group thickness denoted by  $D_{H1}$ . The value of  $D_{H1}$  is measured as the distance between the phosphates and the average hydrocarbon chain boundary of a gel phased lipid with the glycerol backbone aligned parallel to bilayer normal [1.11](#).

$$D_C = D_{H1} - \frac{D_{HH}}{2} = \frac{V_c}{A} \quad (1.11)$$

**iv** By using the (steric) head group thickness  $D_H$  of a monolayer and the half thickness  $D_C$  (Steric bilayer thickness,  $D_{B'}$ ) [1.12](#):

$$D_{B'} = 2(D_C + D_H) \quad (1.12)$$

**v** By using the ratio of volume per lipid  $V_L$  of a monolayer and area per lipid  $A_L$  (Luzzati thickness,  $D_B$ ) [1.13](#):

$$D_B = 2 \frac{V_L}{A_L} \quad (1.13)$$

$D_B$  can also be evaluated from MD simulations, as a function of the box volume  $V_L$  and the water volume  $V_{1w}$  as described in equation:

$$D_B = 2 \frac{(V_b - n_w V_{1w})}{A} \quad (1.14)$$

$$A_L = \frac{Box_X \cdot Box_Y}{N_L} \quad (1.15)$$

Where  $n_w$  is the number of water molecules and  $V_{1w}$  is the volume of water molecules in the simulation box. Various software can be used, which have different ways to define the head groups.

The area per lipid,  $A_L$ , is a vital property for lipid bilayers to describe the lipid phase and the effect of the lipid composition on the lipid bilayer behavior. There are multiple methods and software to calculate the area per lipid. The simplest way to calculate  $A_L$  is to divide the area of the MD simulation box in the XY plane by the number of lipids in one layer as explained in equation 1.15. (The calculation of  $A_L$  are adapted from ref. 3;4) Where  $Box_x$  and  $Box_y$  are the  $X$  and the  $Y$  sides of the simulation box,  $N_L$  is the number of lipids per leaflet. The value of  $A_L$  can also be calculated using the Luzzati thickness  $D_B$  and the volume of lipids  $V_L$ . Although force fields of lipids have regularly been developed to fit with experimental  $A_L$  values, it is important to note that experimental area per lipid values have large errors.<sup>41</sup>

Lipid bilayers tend to be exceedingly dynamic systems whether the system in question is a simple lipid bilayer, a complex combination of lipids in various phases (e.g., nanodomains), or protein complexes floating on membranes. Hence, lateral diffusion is an important parameter to study the behavior of bilayers.<sup>3;7</sup>) Lateral diffusion is experimentally measured by methods such as fluorescence correlation spectroscopy (FCS), fluorescence recovery after photobleaching (FRAP) and Single particle tracking (SPT).<sup>47</sup> In theoretical studies lateral diffusion is computed from MD simulations. In the case of a homogeneous environment, the most common method is to follow the mean squared displacement (MSD) of lipids and estimate the lateral diffusion coefficients according to the Einstein approach.<sup>48</sup> (all equations w.r.t MSD are adapted from ref. 3;4;7)

$$D_{lat} = \lim_{t \rightarrow \infty} \frac{1}{2n} \frac{d}{dt} \langle |\Delta r_{xy}(t)|^2 \rangle = \lim_{t \rightarrow \infty} \frac{1}{2n} \frac{d}{dt} MSD(t) \quad (1.16)$$

$$MSD \equiv \langle (x - x_0)^2 \rangle = \frac{1}{N} \sum_{n=1}^N (x_n(t) - x_n(0))^2 \quad (1.17)$$

Where  $N$  is the number of particles,  $x_{n(0)} = x_n$  is the position of reference (initial position)

of particle  $n$  and  $x_n(t)$  is its position at time  $t$ . The calculation of the diffusion coefficient allows for instance, to check if the fluidity of the simulated lipid bilayer is realistic.

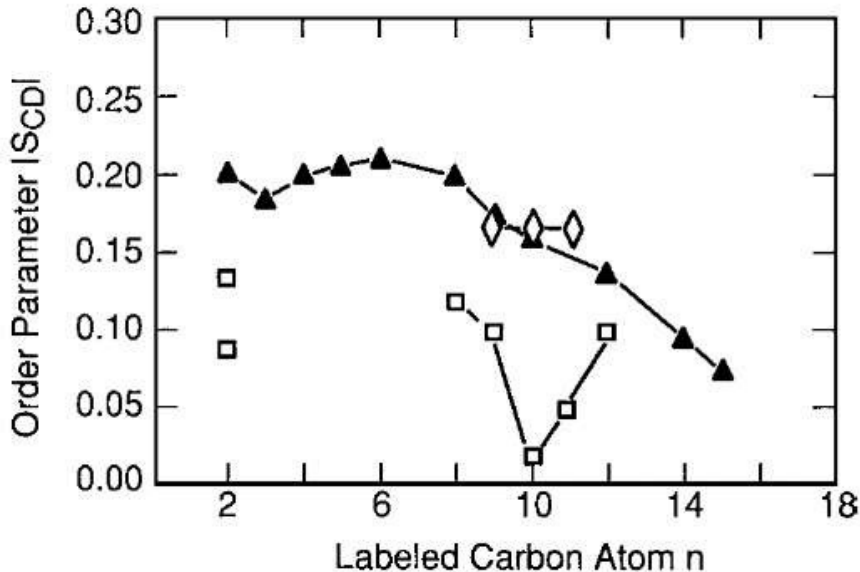


**Figure 1.7:** A Comparison between a sample of a biological membrane and a lipid synthesized by an *in-vivo* method. Values of the deuterium order parameter w.r.t position of the segment for the lipid POPC. Figure adapted from ref. 5;6.

The order parameter,  $S$ , is a dimensionless quantity related to the orientation and the flexibility of lipids in a lipid bilayer and it is defined as shown in [equation 1.18](#).<sup>5;6</sup>

$$S = \frac{3}{2} \langle \cos^2(\theta) \rangle - \frac{1}{2} \quad (1.18)$$

The brackets average the angle  $\theta$  over the simulation time and all lipid molecules. The order parameter is defined by the fluctuation of the angles  $\theta$  defined by the C-H bond vector with respect to the bilayer normal (in membrane MD simulations usually the z-axis). The parameter  $S$  is a value that is usually between  $-0.5$  to  $1.0$ . If a lipid has no preferred orientation (comparable to a lipid tumbling in homogeneous solvent), the value equals  $0.0$ . However, the aforementioned value of “0” corresponds to the perfect order in a bilayer as well with an angle  $\theta = 54.7356^\circ$  (the magic angle). This angle is obtained by solving equation

by substituting  $S = 0$  and considering no average, hence a perfect order. A value of  $S = -0.5$  suggests perfectly ordered acyl chains with all C-atoms in the trans conformation.<sup>41</sup>

An orientation can only be translated in terms of order parameter from dynamical collected data obtained by adequate sampling.

### 1.3.6 A Kirkwood-Buff Derived Force Field for Glycerophospholipids

Before diving into a discussion of KBI derived FF it is worthwhile to lightly review the work done by other FFs. Accurate lipid parameters are essential to derive important data from computer simulations of membranes. There are many lipid parameters sets in use for bilayer simulations, such as the all-atom (AA) CHARMM lipids<sup>49;50</sup>, as well as its united atom (UA) model. The more commonly used UA models are the Berger<sup>51</sup> and GROMOS<sup>41</sup> lipid models. The generalized AMBER<sup>52</sup> force field falls under the polarizable models. A problem of these lipid force fields is the incapability of simulated bilayers to sustain the fluid phase area per lipid value in the NPT ensemble.<sup>53-55</sup> Instead, a dramatic lateral contraction is observed, either resulting in a bilayer that is too densely packed or producing a transition to the gel phase. To compensate, a positive surface tension is used. Finite size effects have been used as an explanation, but some studies found minute reliance of the area per lipid on the size of the system. Especially when long-range electrostatics are considered. It seems the only significant finite size effect is on the lateral diffusion of the lipids, but not on structural properties.<sup>53-55</sup> As an alternative to surface tension, another method to get the accurate area per lipid is to [fix the XY plane area of the box to be a constant \(NPT ensemble\)](#).<sup>39</sup> These parameters have been known to vary with lipid type and hydration level. Furthermore, simulations in the NPAT ensemble do not permit the membrane to stretch and breathe laterally.<sup>53-55</sup>

$$G_{ij} = \int_0^{\infty} [g_{ij}(R) - 1] 4\pi R^2 dR \quad (1.19)$$

Kirkwood-Buff (KB) is a powerful theory of solutions published in 1951.<sup>56</sup> It develops a relationship between the molecular distribution of a multicomponent system in  $\mu VT$  en-

semble to the thermodynamic properties of the said system (e.g., partial molar volumes, derivatives of the chemical potentials and compressibility).<sup>53-55</sup> The KB integrals (KBIs) give the relationship between molecular distributions and thermodynamic properties are described in equation, 1.19. (the equation is adapted from ref. 53)

Here  $g_{ij}(r)$  is the radial distribution function (RDF), or corresponding pair correlation function between species  $i$  and  $j$ . The term  $R$  represents the distance between the matching center of masses for  $i$  and  $j$ . The KBI ( $G_{ij}$ ) calculates the deviation in the distribution of  $j$  molecules around a central  $i$  molecule when compared to that expected for a random distribution of  $j$  molecules.<sup>53-55</sup> If the KB integral between species  $i$  and  $j$  is greater than zero, the affinity between  $i$  and  $j$  is favorable, and a negative value for the KB integral signifies the affinity between the corresponding species to be unfavorable. The KB inversion theory computes the affinity between related species using observable experimental thermodynamic properties of a mixture such as partial molar volumes, isothermal compressibility, and partial vapor pressures. The KB theory is an exact theory without approximations, and it can be used to analyze any stable solution mixture with multiple components. This theory can be applied to any solution regardless of size and complexity of molecules and is ideally suitable for the analysis of computer simulations of solution mixtures. The inversion of KB theory has been mainly applied to two component systems.<sup>53-55</sup>

### 1.3.7 Kirkwood-Buff Derived Force Field for Esters

The forcefield parameters for esters were developed using MD simulations several acetate mixtures. The systems mainly, used include methyl acetate-water, methyl acetate-methanol, methyl acetate-ethanol, ethyl acetate-methanol, methyl propionate-methanol systems to optimize the partial atomic charges for the ester linkage.<sup>53</sup> Since most of these esters are immiscible in aqueous medium alcohol solvents were used as the polar solvents. In this study, all the simulations were carried out at 298 K and 1 atm unless stated otherwise. In this study, a different approach was used to obtain the simulated KB integrals, opposed to the traditional approach. The expression for the finite-volume KB integrals were used,

and then these integrals are linearly extrapolated to obtain a value corresponding to an infinite system. The experimental activities and densities were taken from the literature for all acetate mixtures. A simple mixture rule based on volume fractions was used to obtain the compressibilities. Partial molar volumes were determined from the experimental density data by calculating the excess molar volume. The excess volume and excess molar Gibbs free energy values of acetate-alcohol and acetate-water systems were fitted to the Redlich-Kister equation or NRTL equation.<sup>53-55</sup>

### 1.3.8 Kirkwood-Buff Derived Force Field for Phosphate

The experimental KBI data were not readily available to compare with simulated KBI. Therefore, to obtain experimental KBI values the experimental composition dependent activity and the experimental density data were used after fitting to the Pitzer equation and a polynomial equation. In the case of Dimethyl phosphate salts (DMP) salts the composition dependent osmotic coefficient was used.<sup>53-55</sup> The experimental partial molar volumes are obtained from the experimental densities using previously established standard approaches. The different ions modeled were NaDHP, KDHP, Na<sub>2</sub>MHP, Na<sub>3</sub>PO<sub>4</sub>, NaDMP, LiDMP and KDMP systems. The center of mass radial distribution function was used to calculate the simulated KB integrals. To develop forcefield parameters for phosphate ions, simulated KBI integrals were used to calculate the activity derivatives, excess coordination numbers and partial molar volumes. The translational self-diffusion coefficients were calculated using the mean square fluctuation approach, and dielectric coefficients were calculated by analyzing the mean dipole moment fluctuations.<sup>55</sup>

### 1.3.9 Kirkwood-Buff Derived Force Field for Polyols

To develop force field parameters for polyols, KB analysis were performed for experimental data of six binary mixtures, inversion of KB theory. The fitting constants for the excess molar volumes (VmE) and excess molar Gibbs energies (GmE) for glycerol/water (GLY/H<sub>2</sub>O) and 1,2-ethanediol/water (EDL/H<sub>2</sub>O) systems were obtained. Using the raw activity co-

efficients for the 1, 2-ethanediol-methanol (EDL/MOH) mixture, GmE was calculated as a function of composition and fitted using Redlich-Kister polynomial. Water activity data for 1,2-propanediol-water (1,2-PDL/HOH) and 1,3-propanediol-water (1,3-PDL/HOH) mixtures were used to calculate GmE for binary mixtures. The torsion angle parameters were parameterized to reproduce experimentally, and quantum mechanically, 150 obtained conformation energies for GLY and EDL. The parameters obtained for H-O-C-C and O-C-C-O angles of EDL were then also used in parameterizing 1,2-propanediol. The partial atomic charges were varied until they reproduced experimental KBIs in the condensed phase as a function of composition. <sup>54</sup>.

# Chapter 2

## Single Lipid Simulations

### 2.1 Introduction

The [fundamentals which determine](#) lipid conformations in bilayer membranes have been clearly understood from x-ray crystal structures for a range of different phospholipids, glycolipids, diglycerides, and ceramides.<sup>57</sup>

The bilayer crystal structure of phosphoglycerolipids is characterized by the backbone (glycerol) dihedrals, and by which of the  $sn-1$  and  $sn-2$  chains is the prominent one advancing directly into the bilayer from its connection to the glycerol. To accomplish parallel chain packing, the chain that did not advance to the chain is then bent by  $90^\circ$  at the backbone. The polar head group is bent approximately forming an angle of  $\sim 90^\circ$  with the bilayer normal (z-axis of a simulation box) and stays almost parallel to the bilayer.<sup>58-60</sup>

The configurational disorder from chains arises from energetically disallowed skew conformations. Eclipsed conformations occur in some glycerol backbone torsion angles and in C-C torsion angles of the lipid head groups.<sup>59</sup>

Experimental data on the dynamic lipid structures that occur in fluid bilayer membranes come mostly from magnetic resonance studies. Generally, the  $sn-1$  and  $sn-2$  acyl chains are in-equivalent in fluid bilayers ( $L$ ) with  $sn-1$  as the leading chain.<sup>61</sup>

According to NMR experiments of phospholipid micelles glycerol backbone has two stable

conformers.<sup>60</sup> However, these (conformers) include a conformationally forbidden nonplanar ester carboxyl and a relatively high-energy glycerol backbone configuration.<sup>57</sup> This, therefore, also suggests the presence of a limited number of interconverting conformers. A survey of many popular lipid force fields as demonstrated in this study illustrates the need for better agreement with NMR data on the glycerol backbone and choline head group. Although it may seem like an oversimplification to describe the dynamic structure of fluid lipid bilayers has a limited number of molecular configurations, and provide a framework to understand the behavior of biological membranes, which are both highly dynamic and highly ordered.<sup>57</sup>

The function of acyl chains in a 1-palmitoyl-2-oleoylphosphatidylcholine (POPC) lipid bilayer is relatively well known. Importantly, the structural parameters for the glycerol backbone are equivalent for numerous lipid molecules found in living membranes. Hence glycerol backbone parameters can be appropriated for phosphatidylcholine (PC), phosphatidylethanolamine (PE), and phosphatidylglycerol (PG) in numerous environments. The structural parameters for the choline head group are comparable in model membranes and real cells (mouse fibroblast L-M cell).<sup>62</sup>

The experimental C-H bond order parameters and gauche-trans isomerism are frequently compared between experiment and simulations for the acyl chains, for the glycerol backbone (*C12*, *C13*, and *C34*) and choline (*C5* and *C6*) section.<sup>63</sup>

These are among the key parameters used in efforts to obtain lipid structures from experimental data. Most importantly, the structures representative of a simulation that replicate these order parameters will axiomatically encompass a rendition of the experimental studies. This type of simulations can be considered as a precise elucidation of a lipid bilayer at the atomic scale. A few studies have compared the glycerol backbone and choline head group order parameters and gauche-trans isomerism between simulations and experiments.<sup>57;62;63</sup>

In addition to fully hydrated single component lipid bilayers, the glycerol backbone and choline order parameters have been measured under a large number of changing conditions: hydration level, cholesterol content, ion concentration, temperature, charged lipid content, charged surfactant content, drug molecule concentration, and protein content.<sup>62</sup>

Existence of these data allows the comparison of structural responses to varying condi-

tions between simulations and experiments.<sup>60;62;64</sup>

Hence, validate the simulated models and interpret the original experiments. The glycerol backbone can be regarded as the core of the phospholipid molecule to which the three substituent chains, the head group, and both acyl chains are linked. The head group is attached to atom *C12* of the glycerol by a phosphate ester bond, and the two acyl chains are linked via ester or ether bonds to carbon atoms *C13* and *C34* of the glycerol group.<sup>63</sup> Since the two acyl chains in lipid bilayers and lipid aggregates are stacked in parallel, an issue arises if this chain stacking necessitates a specific conformation of the glycerol group. This matter is resolved by <sup>1</sup>H high-resolution NMR using different phospholipids and different solvents. The prevalent lipid aggregate in this type of study is the small micelle and the monomeric lipid molecule in equilibrium with the micelle. Both types give rise to high-resolution NMR spectra with lines adequately narrow to demonstrate spin-spin interactions. Conformational data is obtained from vicinal <sup>1</sup>H-<sup>1</sup>H spin coupling.<sup>63;65</sup>

The NMR data taken with micelles and monomeric solutions is compared with respect to the single-crystal structure of related lipids and with data in the literature acquired with NMR methods.

A comparison between accurate X-ray single-crystal structures and structural data resulting from liquid-crystalline, partly disordered systems have shed light on the question to what degree the minimum energy conformation of the glycerophospholipids in the single crystals are reserved in a liquid-crystalline bilayer assembly. In this study, the most relevant experimental data for the glycerol backbone gauche-trans isomerization data is reviewed for phosphatidylcholine single lipid molecule.<sup>65</sup>

The experimental value is compared to KBFF simulated model and the dihedral parameters that give the most realistic glycerol backbone conformation is identified.

## 2.2 Parameter Development

The bond, angle and torsion parameters are adopted from previous KBFF models for glycerol, ester, and phosphate groups present on the glycerophospholipid molecule.<sup>53-55</sup> Torsion

angle parameters were parameterized to reproduce experimental data.<sup>63</sup> The torsion angle parameters used in this study are summarized in Table 2.1.<sup>63</sup> Non-bonded interactions are treated with a Lennard Jones (LJ) 6–12 and Coulomb potential. The  $\sigma$  and  $\epsilon$  parameters for the LJ term of the carbon atoms and the effective partial atomic charges were also adopted from the new version of KBFF.

**Table 2.1:** *Torsion angles parameters used for the glycerol backbone. Dihedral angles were defined according to Figure 2.1, where the phase shift  $\delta$  is taken to be  $-60$  and  $+60$  for all angles*

model	angle	$K_\psi$ (kJ/mol)	$\delta$
POPC	O-C-C-O	-3	-60.0
	11-12-13-14	-8	60.0
POPC	O-C-C-O	-3	60.0
	14-13-34-35	-8	-60.0

## 2.3 Molecular Dynamics Simulations

The five different systems that were simulated with different force fields (KBFF, GROMOS54a6, CHARMM36, OPLS, SLIPID).<sup>39;49;62?</sup> All five lipids were single lipids constituting a POPC lipid molecule in water. Water is added to each system to get above 30% level of hydration as described in experiment. Different FFs are usually optimized to be used with a specific water model. Hence different FFs were used with the corresponding water models, KBFF, GROMOS54a6, CHARMM36, OPLS, SLIPID.<sup>62</sup> furthermore eight different lipids (POPC, POPE, POPS, DOPC, DOPE, DOPS, DPPC, DMPC) were simulated with a hydration level of 30%. All simulations were performed using the GROMACS package.<sup>66</sup> All lipid systems were placed in a rectangular box under periodic boundary conditions. The lipids and water (solvent) were independently coupled to an external water bath with a coupling constant ( $\tau_T$ ) of 0.1 ps at an external temperature of 300 K, to maintain the temperature of the system. A constant pressure at 1 bar in both lateral and normal by a weakly coupled semi-isotropic pressure bath.<sup>67</sup> The isothermal compressibility of  $4.6 \times 10^{-5}$  and a coupling constant ( $\tau_p$ ) of 1 ps was used. The covalent bonds (length) in the lipid molecule was con-

strained using LINCS algorithm.<sup>68</sup> The water molecules were modeled using an appropriate water model (SPC,SPC/E,TIP3).<sup>69–72</sup> The Non-bonded interactions were evaluated with a Verlet scheme at a cut-off of 1.0 nm.<sup>70</sup> The Particle Mesh Ewald method was used to calculate the electrostatic interactions between molecules.<sup>73</sup> Each system was energy minimized using Steepest descent method at 300 k and equilibrated. After equilibration, all systems were simulated for 500 ns, every 1000 steps, with a 0.2 ps time frame.<sup>65</sup>

**Table 2.2:** *The gauche and trans percentages of the glycerol backbone POPC single lipid*

Forcefield	angle	$-g$ $\exp(0.38)$	$+g$ $\exp(0.61)$	$t$ $\exp(0.01)$
KBFF	O-C-C-O	0.35	0.64	0.01
	14 – 13 – 34 – 35			
CHARMM36	O-C-C-O	0.26	0.58	0.16
	14 – 13 – 34 – 35			
GROMOS54a6	O-C-C-O	0.48	0.09	0.43
	14 – 13 – 34 – 35			
OPLS	O-C-C-O	0.40	0.16	0.44
	14 – 13 – 34 – 35			
SLIPID	O-C-C-O	0.31	0.49	0.20
	14 – 13 – 34 – 35			

## 2.4 Results and Discussion

The g/t isomerization of glycerol backbone was calculated using dihedral angle population histograms, where the area under the histograms corresponding to +g, –g and t were determined by trapezoid rule as shown in table 2.3. The atom numbering is described in Figure 2.1. From these atoms the glycerol backbone dihedral angle with experimental data is O – 14, C – 13, C – 34, O – 35, where the first letter describes the atom, and the following number describes the position of that atom w.r.t to a POPC lipid molecule.

Furthermore, the time vs dihedral angle plots clearly show the glycerol backbone spends the maximum time in +g and –g conformations. The Figure 2.12.2, A and B respectively shows O – 11, C – 12, C – 13, O – 14 and O – 14, C – 13, C – 34, O – 35 glycerol back bone

**Table 2.3:** *The gauche and trans percentages of the glycerol backbone POPC single lipid*

lipid	angle	$-g$	$+g$	<b>t</b>
POPC	O-C-C-O	0.29	0.70	0.01
	14 - 13 - 34 - 35			
POPE	O-C-C-O	0.30	0.69	0.01
	14 - 13 - 34 - 35			
POPS	O-C-C-O	0.31	0.68	0.01
	14 - 13 - 34 - 35			
DOPC	O-C-C-O	0.27	0.72	0.01
	14 - 13 - 34 - 35			
DOPE	O-C-C-O	0.27	0.72	0.01
	14 - 13 - 34 - 35			
DOPS	O-C-C-O	0.28	0.71	0.01
	14 - 13 - 34 - 35			
DPPC	O-C-C-O	0.26	0.73	0.01
	14 - 13 - 34 - 35			
DMPC	O-C-C-O	0.22	0.77	0.01
	14 - 13 - 34 - 35			

dihedral angles. In each case the respective dihedral angle is compared with single lipid with respect to the bilayer. As shown in Figure 2.12.2, A and B, both dihedral angles associated with glycerol backbone sample  $-g$  and  $+g$  conformations in the complete simulation time which is in good agreement with the experimental data.

These observations are further established by the dihedral PMF of the angle  $O14C13C34O35$ , as shown in Figure 2.2, where the free energy minimums of the dihedral angle are at  $+g$  and  $-g$  conformations. The behavior observed in bilayers will be thoroughly discussed in chapter 3. Furthermore, the PMF of dihedral angles from choline head group to glycerol backbone and two dihedral PMF from aliphatic chain (atoms of acyl chain attached to the glycerol moiety) is shown in Figure 2.3. These indicate that the single lipid molecule dihedral angles are in minima values that correspond with experiment.<sup>65</sup>

The cis double bond represented by atoms 24 and 25 in Figure 2.1 should be in a planar conformation. The PMF of the cis double bond is indeed planar as shown in Figure 2.4. Furthermore, the PMF is compared to the cis double bond PMF of other FFs. According to Figure 2.4 all FFs seem to be in good agreement.

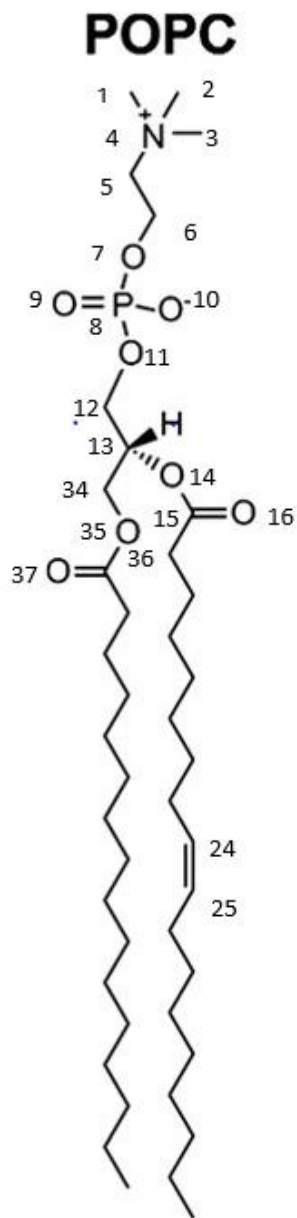


**Figure 2.1:** A labeled diagram for POPC lipid

The diffusion for the single lipid molecules were calculated to observe how well the lipid molecules have diffused in 3D space. According to the results in table 2.4 the molecules have sampled many conformations and sampled translational space to a satisfactory level. Furthermore, table 2.5 shows the diffusion coefficient (single POPC in water) for different FFs.

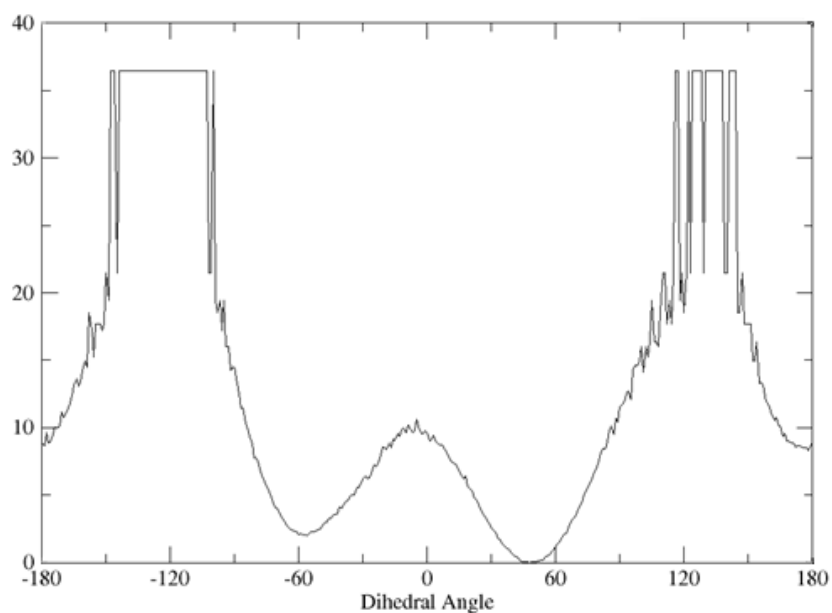


**Figure 2.2:** The PMF ( $\text{kJmol}^{-1}$ ;  $y$ -axis) of  $O14C13C34O35$  dihedral angle ( $x$ -axis)

**Table 2.4:** Single lipid molecules diffusion coefficient for various lipids

Lipid	Diffusion Coefficient $D(\text{cm}^2\text{s}^{-1}) \times 10^{-5} \pm 0.1 \times 10^{-5}$
POPC	5.68
POPE	5.16
POPS	6.40
DOPC	5.20
DOPE	6.31
DOPS	4.25
DPPC	1.37
DMPC	1.25

**Table 2.5:** POPC single lipid molecule diffusion coefficient for different FFs

Forcefield	Diffusion Coefficient $D(\text{cm}^2\text{s}^{-1}) \times 10^{-5} \pm 0.1 \times 10^{-5}$
KBFF	5.68
CHARMM36	7.38
GROMOS54a6	1.12
OPLS	9.75
SLIPID	1.72

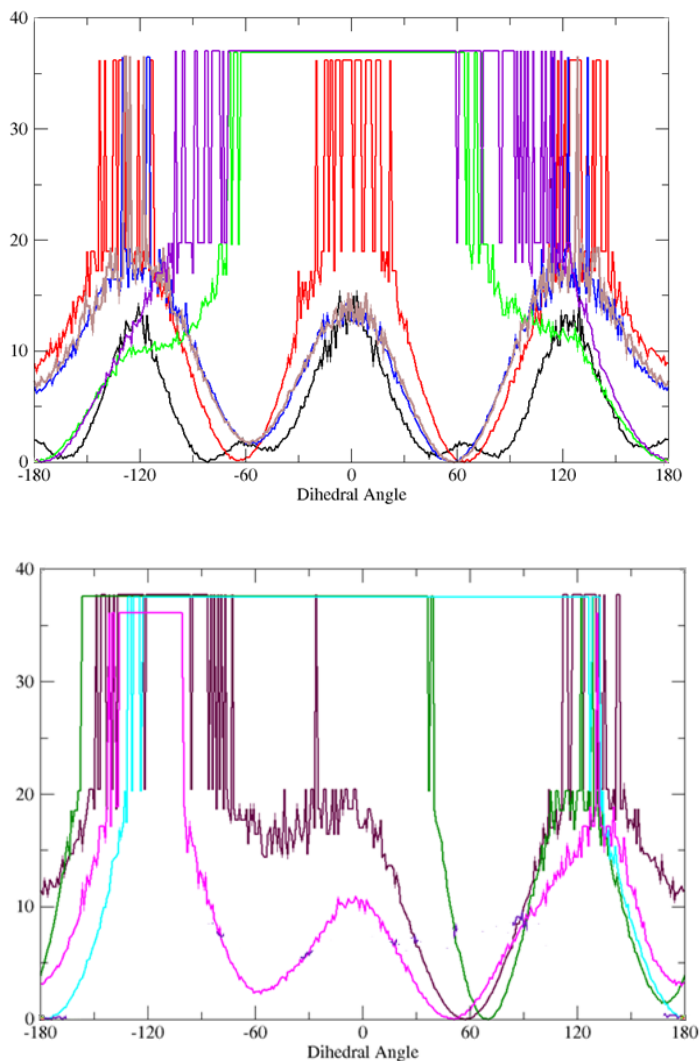


**Figure 2.3:** The PMF ( $\text{kJmol}^{-1}$ ;  $y$ -axis) of dihedral angles ( $x$ -axis) consisting of atoms,  $C3N4C5C6$  (black),  $C5C6O7P8$  (red),  $C6O7P8O11$  (blue),  $O7P8O11C12$  (brown),  $P8O11C12C13$  (violet), in (a) and  $O11C12C13O14$  (maroon),  $C12C13O14C15$  (green),  $C13O14C15O16$  (cyan),  $O14C13C34O35$  (magenta),  $O14C15C17C18$  (indigo) in (b)

## 2.5 Conclusion

Non polarizable FFs were developed for POPC lipid molecule to successfully reproduce experimental data. Compared to other classical FFs KBFF reproduces experimental data very well. Therefore, the next step is to use these FF parameters and simulate pure lipid bilayers and observe if bilayer physical properties can be successfully reproduced.

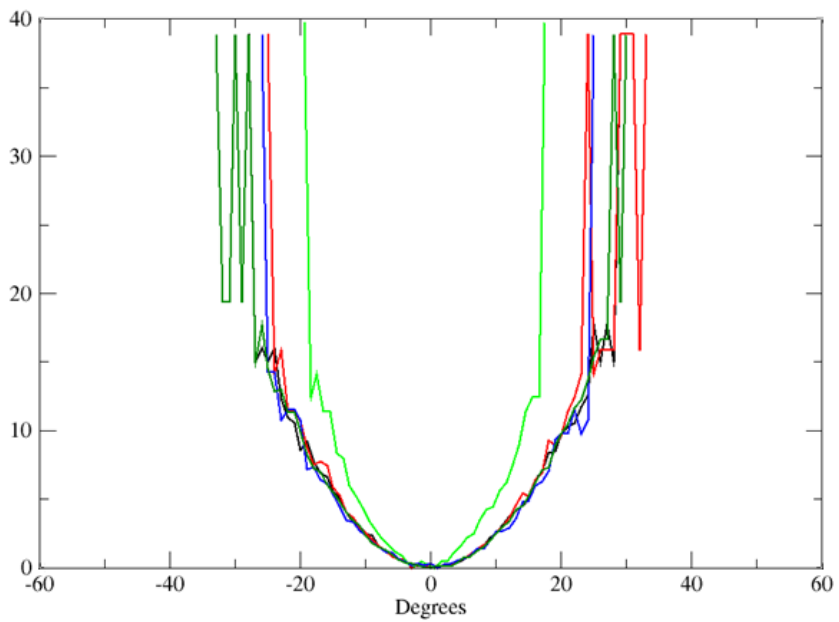


**Figure 2.4:** The PMF ( $\text{kJmol}^{-1}$ ;  $y$ -axis) of dihedral angle ( $x$ -axis) at *cis* double bond in the POPC (single lipid) acyl chain. The FFs are CHARMM36(black), GROMOS (red), OPLS (green), SLIPID (blue)

# Chapter 3

## Pure Phospholipid bilayers

### Simulations

#### 3.1 Introduction

Pure phospholipid bilayers are thoroughly explored to model biologically pertinent membranes. The most studied lipid phase is the fluid phase, because it is physiologically relevant. In  $L_{\alpha}$  the acyl chains have greater flexibility resulting in a disordered and fluid membrane. The disorder nature of the membrane hinders studying the lipid systems at atomic level. Hence using a theoretical approach, such as MD simulations, can aid in understanding the static and dynamic properties of lipids.<sup>74</sup>

Previous work using MD simulations helped to understand critical aspects in important mechanisms, such as the formation of lipid vesicles, pore formation in membranes, ion permeation through membranes, lipid flip-flop and self-assembly of lipids into a bilayer.<sup>75</sup>

Membrane MD simulations heavily rely on how the FF treats inter-atomic interactions. Researches are consistently improving lipid FF parameters, but are not able to successfully reproduce static and dynamic properties of phosphatidylcholine lipid bilayers. it is important to note phosphatidylcholine lipids are a major component of biologically relevant membranes.<sup>76</sup>

The parameters discussed in chapter 1 for phosphate, choline and parameters discussed in chapter 2 for the glycerol moiety is used. Various phospholipid bilayers at  $L_\alpha$  are modeled using the aforementioned parameter set. Many researchers reproduce  $A_L$  to validate the accuracy of the lipid FF parameters. The experimental  $A_L$  values are not calculated directly but deduced from NMR order parameters, using EDPs obtained from X-ray studies and many other experimental methods. Hence there is some variation in experimental  $A_L$  values.<sup>39;76;77</sup>

Although authors of previous work use different parameters, the area per lipid achieved by MD simulations is in a **narrow** range, Furthermore they are independent of the length of the simulation and the time to which the specific system was equilibrated. The area per lipid in simulations of bilayer systems fluctuate under periodic boundary conditions.<sup>39</sup>

Although the  $A_L$  values are in a small range the methods used to calculate long-range electrostatics is are different. The errors created by undulations of the membrane and artifacts in experimental measurements rarely get any attention.<sup>76;78</sup>

## 3.2 Methods

### 3.2.1 Simulation System

**Table 3.1:** *Description of simulated systems*

Lipid Type	Lipid Molecules	Water Molecules	Simulation Time/ $\mu s$
POPC	128	5941	1.0
POPE	128	5943	1.0
POPS	128	5941	1.0
DOPC	128	6040	1.0
DOPE	128	6041	1.0
DOPS	128	6040	1.0

The eight different systems that were simulated are described in Table 3.1. All eight lipids were pure bilayers constituting sixty four lipids in each leaflet. The preferred level of hydration in the  $L_\alpha$  phase is reached by adding about 35 – 40  $H_2O$  molecules per lipid.

### 3.2.2 Simulation Parameters

All simulations were performed using the GROMACS package.<sup>79</sup> All lipid systems were placed in a rectangular box under periodic boundary conditions. The lipids and water (solvent) were independently coupled to an external water bath with a coupling constant ( $\tau_T$ ) of 0.1 ps at an external temperature of 300 K, to maintain the temperature of the system.<sup>39;76</sup> A constant pressure at 1 bar in both lateral and normal by a weakly coupled semi-isotropic pressure bath. The isothermal compressibility of  $4.6 \times 10^{-5}$  and a coupling constant ( $\tau_p$ ) of 1ps was used. The covalent bonds (length) in the lipid molecule was constrained using LINCS algorithm.<sup>80</sup> The water molecules were modeled using the simple point charge extended (SPC/E) water model.<sup>81;82</sup> The Non-bonded interactions were evaluated with a Verlet scheme at a cut-off of 1.0 nm. The Particle Mesh Ewald method was used to calculate the electrostatic interactions between molecules.<sup>80</sup> Each system was energy minimized using Steepest descent method at 300k and equilibrated. After equilibration, all systems were simulated for  $1.0\mu s$ , every 1000 steps, with a 0.2 ps time frame.<sup>51</sup>

## 3.3 Results

### 3.3.1 Area per Lipid( $A_L$ )

**Table 3.2:** Comparison of simulated area per lipid and experimental area per lipid

Lipid Type	Area/Lipid( $\text{nm}^2$ ) Simulated	Area/Lipid( $\text{nm}^2$ ) Experimental (Adapted from ref 8)
POPC	0.64	0.65
POPE	0.63	–
POPS	0.67	–
DOPC	0.67	0.67
DOPE	0.66	–
DOPS	0.68	0.69
DPPC	0.62	0.63
DMPC	0.60	0.61

As described in chapter 2, in simulations  $A_L$  is calculated by lateral area of the simulation

box divided by the number of lipids in each leaflet. The time averaged values for  $A_L$  is presented in Table 3.2 along with respective experimental values. The parameters used are described in chapter 2. The forcefield parameters used yields  $A_L$  value are about 0.5% higher than experiment.

### 3.3.2 Volume per Lipid( $V_L$ )

The time averaged  $V_L$  values are reported in table 3.3 together with experimental values. The simulated  $V_L$  value of POPC, DOPC, DPPC, DMPC is about 0.6% higher than experimental values.

**Table 3.3:** Comparison of simulated volume per lipid and experimental volume per lipid

Lipid Type	Volume/Lipid( $\text{nm}^3$ ) Simulated	Volume/Lipid( $\text{nm}^3$ ) Experimental (Adapted from ref 8)
POPC	$1.196 \pm 0.002$	$1.192 \pm 0.003$
POPE	1.183	–
POPS	1.198	–
DOPC	$1.312 \pm 0.001$	$1.303 \pm 0.002$
DOPE	1.298	–
DOPS	1.316	–
DPPC	$1.233 \pm 0.002$	$1.229 \pm 0.001$
DMPC	$1.112 \pm 0.003$	$1.101 \pm 0.001$

### 3.3.3 Electron Density Profile(EDP)

**Table 3.4:** Comparison of simulated  $D_{HH}$  and experimental  $D_{HH}$

Lipid Type	$D_{HH}$ (nm) Simulated	$D_{HH}$ (nm) Experimental (Adapted from ref 8)
POPC	$3.820 \pm 0.003$	$3.700 \pm 0.005$
POPE	$3.830 \pm 0.003$	$3.840 \pm 0.005$
POPS	$3.850 \pm 0.003$	$3.900 \pm 0.003$
DOPC	$3.660 \pm 0.004$	$3.670 \pm 0.006$
DOPE	$3.650 \pm 0.004$	–
DOPS	$3.770 \pm 0.004$	–
DPPC	$4.060 \pm 0.006$	$3.800 \pm 0.003$
DMPC	$3.600 \pm 0.003$	$3.530 \pm 0.002$

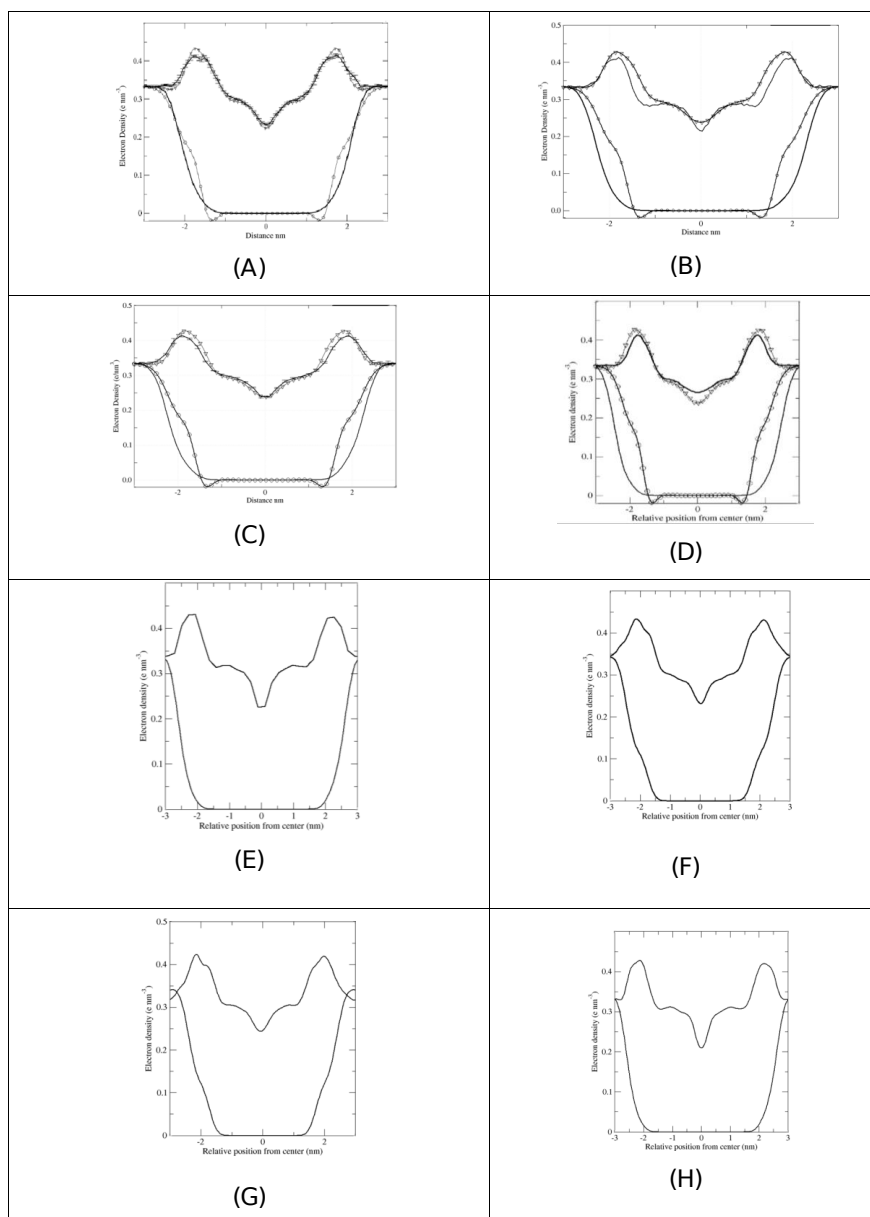
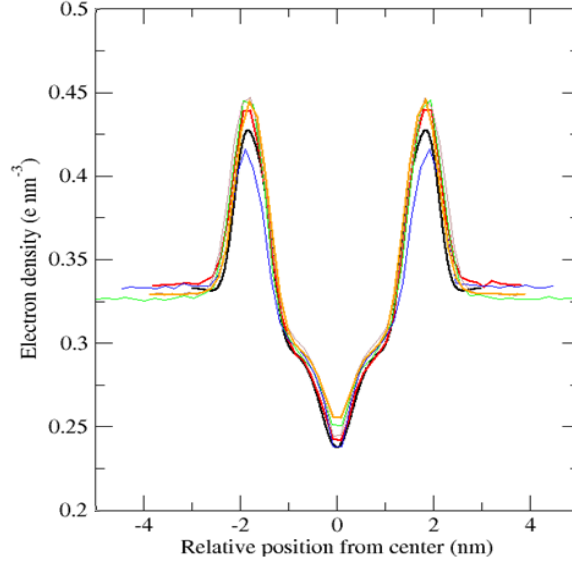
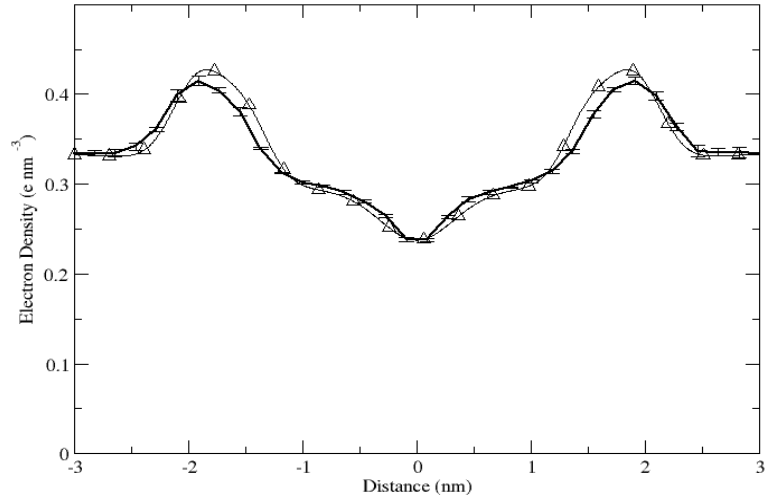


**Figure 3.1:** Total EDP of DMPC (A), DOPC (B), POPC (C), DPPC (D), DOPE (E), DOPS (F), POPE (G), POPS (H), in black line. The Density of water is included (in black line; to complement lipid EDP). All corresponding experimental curves and models (of total electron density) developed from experimental data are in black downward triangles. All corresponding experimental curves of water developed from experimental data are in a black circle.<sup>7</sup>

The Electron density profile for DOPC, and POPC bilayers are shown in figure 3.1 A and B, respectively. Electron density profile are a straightforward, popular way do a qualitative comparison with experiment. The main contributor to the two major peaks in the density



(A)



(B)

**Figure 3.2:** EDP of POPC in comparison of FFs (A; experiment-black, CHARM36-red, GROMOS54A7-green, KBFF-blue, OPLSAA-grey, SLIPID-orange) POPC 512 lipid systems in water (B;black line). The corresponding experimental curves and models (of total electron density) developed from experimental data are in black upward triangles.<sup>7</sup>

profiles are the phosphorus atoms in the head group, the most electron-dense atoms in the bilayers. The thickness  $D_{HH}$  of a bilayer is commonly taken as the distance between the

two phosphate peaks (or head group peaks). Alternatively, the Luzzati thickness  $D_B$  can be used for thickness as well. The values of  $D_{HH}$  observed in the simulations are reported in table 3.4. The simulated values have good agreement with the values obtained from experimental studies of lipid bilayers in  $L_\alpha$  phase.  $D_{HH}$  obtained from simulations are within 1% of those measured experimentally as listed in table 3.4. The EDP profile of simulated POPC is compared to other popular FFs. The  $D_{HH}$  of the simulated profile is slightly lower than the experimental model and other FFs. Therefore, further work needs to be carried out to study this phenomenon. The POPC bilayer EDP with 512 lipids is in good agreement with the experimental profile as shown in figure 3.1 B.

### 3.3.4 Deuterium Order Parameters( $S_{CD}$ )

As explained in chapter-1 the  $S_{cd}$  of acyl chains can be calculated using simulations. The calculated acyl chain  $S_{cd}$  for lipid bilayers POPC, POPS, POPE, DOPC, DOPE, DOPS is shown in figure 3.3 and figure 3.4 The acyl chain order parameters seem to be in good agreement with experiment.

### 3.3.5 Diffusion Coefficient

**Table 3.5:** Diffusion coefficient( $D$ ) for lipid bilayer systems. A comparison of simulated  $D(\text{cm}^2\text{S}^{-1} \times 10^{-8})$  and experimental  $D(\text{cm}^2\text{S}^{-1} \times 10^{-8})$

Lipid Type	Simulated $D(\text{cm}^2\text{S}^{-1} \times 10^{-8})$	Experimental $D(\text{cm}^2\text{S}^{-1} \times 10^{-8})$ (Adapted from ref 8)
POPC	$8.4 \pm 0.002$	7.8, 8.9, 8.6
POPS	$6.9 \pm 0.001$	–
POPS	$11.5 \pm 0.001$	–
DOPC	$11.6 \pm 0.002$	9.3
DOPE	$22.8 \pm 0.003$	–
DOPS	$10.3 \pm 0.004$	–
DMPC	$4.7 \pm 0.001$	5.5
DMPC	$1.2 \pm 0.002$	1.6

The diffusion coefficient of the lipid bilayer systems was calculated and compared to experiment. As shown in table 3.5 the experimental values and simulated values seem to be

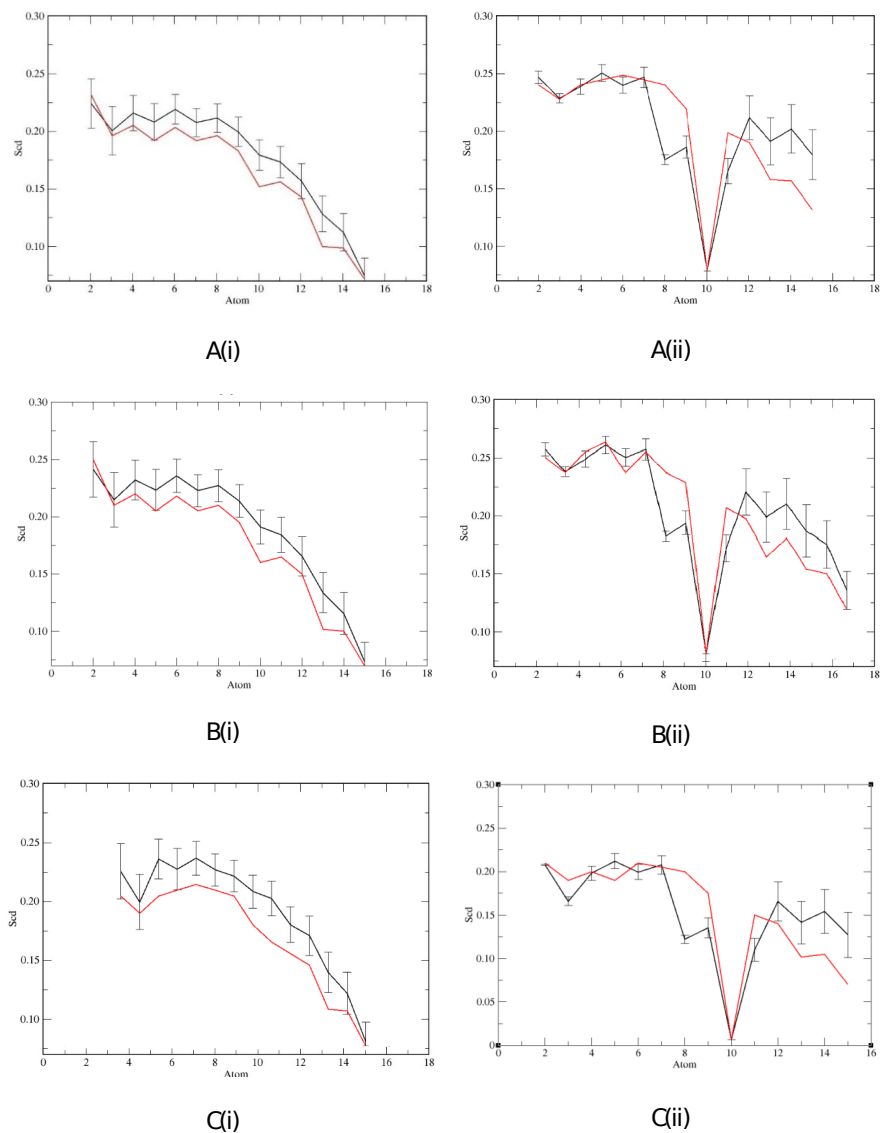


**Figure 3.3:** Acyl chain  $S_{cd}$  of POPC  $sn - 1$ ,  $sn - 2$  (A-i, ii), POPE  $sn - 1$ ,  $sn - 2$  (B-i, ii), POPS  $sn - 1$ ,  $sn - 2$  (C-i, ii), compared to that of experiment. The experimental values are adopted from ref 8;9

**Table 3.6:** Diffusion coefficient( $D$ ) POPC for Different FFs

Forcefield	Simulated $D(\text{cm}^2\text{s}^{-1} \times 10^{-8})$
KBFF	$8.4 \pm 0.002$
GROMOS54a6	$8.38 \pm 0.004$
CHARMM36	$7.82 \pm 0.002$
OPLS	$9.65 \pm 0.001$
SLIPID	$7.68 \pm 0.003$

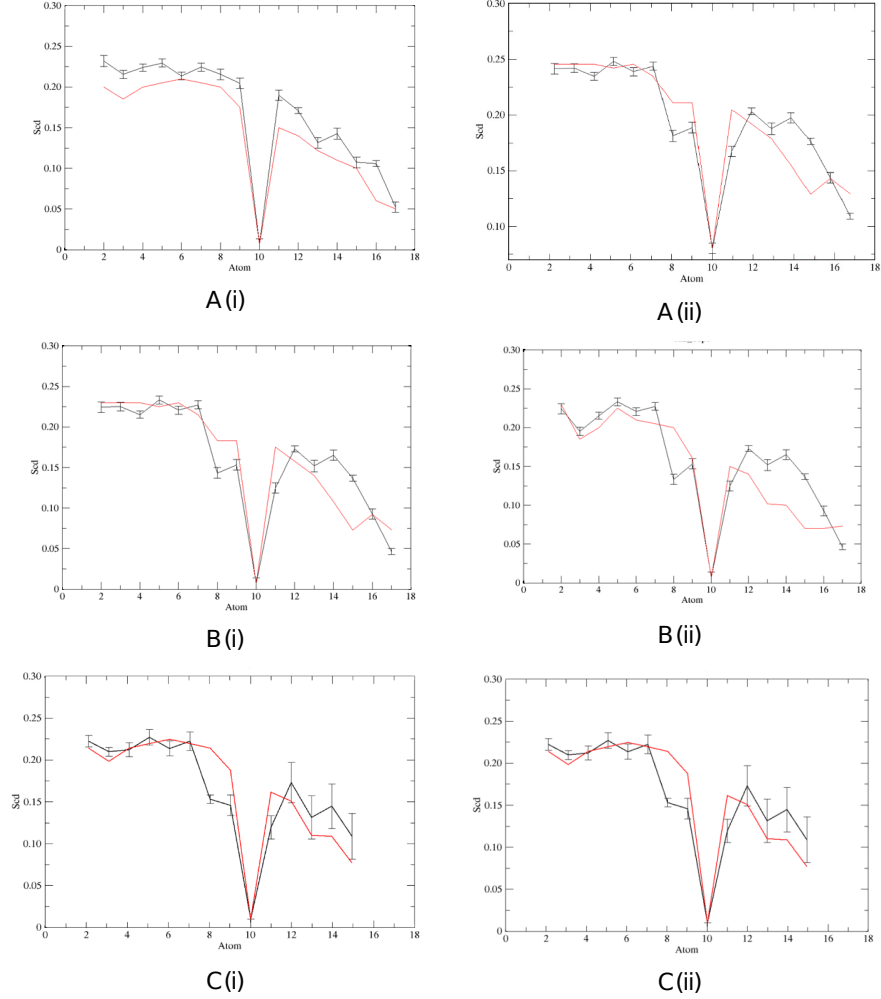


**Figure 3.4:** Acyl chain  $S_{cd}$  of (A-i, ii), DOPE  $sn-1$ ,  $sn-2$  (B-i, ii), DOPS  $sn-1$ ,  $sn-2$  (C-i, ii), compared to that of experiment. The experimental values are adopted from ref 8;9

in good agreement. Furthermore, a comparison of the diffusion coefficient values of popular FF to KBFF of POPC bilayer is shown in table 3.6.

### 3.4 Discussion

Overall, the KBFF force field parameters have been shown to represent a range of phosphoglycerolipids in  $L_\alpha$  phase and successfully reproduce a range of structural properties. These include the  $A_L$ ,  $V_L$ , the deuterium order parameters (of glycerol backbone and acyl chains), and the hydration properties, are in close agreement with experiment. The valida-

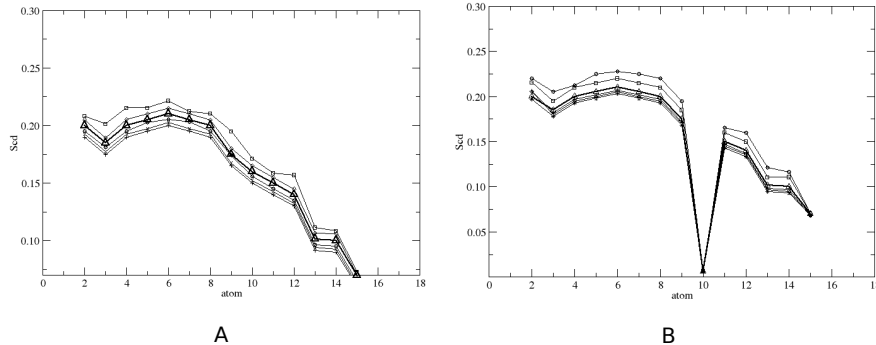


**Figure 3.5:** Acyl chain  $S_{cd}$   $sn - 1$ ,  $sn - 2$  (A, B) of POPC 512 lipid system compared to that of experimental. The upward triangle is experimental  $S_{cd}$  values, the star is  $S_{cd}$  values at 200 ns, the cross is  $S_{cd}$  values at 400 ns, the circle is  $S_{cd}$  values at 600 ns, the square is  $S_{cd}$  values at 800 ns, the diamond is  $S_{cd}$  values at 1000 ns

tion of membrane simulations in  $L_\alpha$  phase is, a difficult task. Phospholipids are amphipathic molecules, where the central polar group glycerol is attached to two or three, hydrophobic acyl chains and to a polar head-group. Consequently, the phase behavior of a lipid bilayer is the outcome of a fine-drawn equilibrium between inter- and intra- molecular forces as well as the balance among interactions within the head-group and acyl chain regions. The compactness of a lipid bilayer additionally means that structure and dynamics are well correlated. For example, in  $L_\beta$ , lipids pack more tightly and highly ordered compared to  $L_\alpha$  phase. In simulations,  $A_L$  depends on sampling time, the size of the system, and the methodology. Therefore,  $A_L$  is just one of many in a range of properties that need to be considered during the validation of force field parameters for lipids. In this work, a collection of structural properties ( $A_L$ ,  $D_{HH}$  and  $S_{CD}$ , conformation of the acyl chains, and orientation of the head-groups) were used to validate the KBFF parameter set. As shown a good agreement was found with experiment for all the discussed structural properties. The Berendsen weak-coupling method was used in this study to maintain constant temperature and pressure. The Berendsen thermostat and barostat do not give rise to an exact NPT ensemble. Although the long-time averages are correct, Berendsen weak-coupling technique may suppress short-time fluctuations in the temperature and the pressure. Hence, it should be noted that, while the temperature and the pressure fluctuations in the simulations occur on a 1 – 10 ps time

scale, the fluctuations in properties occur on a 10 – 100 ns time scale. Thus, fluctuations in structural properties are not likely to be greatly affected or biased by the relaxation time applied in the weak coupling of temperature ( $\tau_T$  0.1 ps) and pressure ( $\tau_P$  0.1 ps). Other factors that could lead to a small over-estimation of the fluctuations in structural properties consist of the containment of the fluctuations due to the size of the system and the time scale over which the fluctuations were accumulated. The structural properties such as  $A_L$  are key to validating force field parameters. The local properties, such as the rotameric states are similarly important. The incidence of rotamers and sequences of rotamers in the acyl chains are used to determine if the simulations replicate the correct phase of the lipid. The percentage of gauche rotamers rises in the gel  $\rightarrow$  liquid crystal phase transition of lipids. The occurrence of all-trans acyl chains is distinctive to the gel phase.

The simulation results together with the experimental values suggest the lipids to be in in the  $L_\alpha$  phase. The incidence of e.g., bonds and  $gg$  sequences in the saturated lipids suggest good agreement with measurements inferred from spectroscopic method. The  $S_{CD}$  is highly correlated to  $A_L$ , with higher ordering for bilayers that are laterally very small. Order values are very susceptible to go to  $t$  energy transfer of the acyl dihedral torsions. The results agree with the previously reported experiments. A special case is the carbon  $C2$  in the  $sn-2$  chain, with  $S_{CD}$  which is split into a much lower 0.21 and 0.09. In the  $sn-1$  chain however the  $C2$  always seem to be around  $S_{CD}$  of 0.2. Replicating the splitting on  $sn-2$  chain  $C2$  would necessitate withdrawing from the united-atom model and explicitly including the C-D bonds. Regardless Of the non-existence of the deuterium, the results show that  $S_{CD}$  can be correctly obtained using the united-atom method.

In all lipid systems, the  $S_{CD}$  values are lower than 0.25, which implies disordered acyl chains. The variations and magnitudes of  $S_{CD}$  values for all the systems containing lipid bilayers are similar to the corresponding experimental values. In the case of POPC lipid bilayer system, the simulation reproduced the both subtle and distinct differences between palmitoyl ( $sn-1$ ) and oleoyl ( $sn-2$ ) chain  $S_{CD}$  values which are observed experimentally. The  $sn-1$  chain demonstrates an uninterrupted decline in  $S_{CD}$  values, which is distinctive of saturated chains. The  $S_{CD}$  values of the  $sn-2$  chain has a distinctive drop, consequent

to the double bond between carbons 9 and 10. Furthermore, the *sn*-2 chain is clearly more disordered compared to the saturated chain. The  $S_{CD}$  values of the oleoyl chains in DOPC lipid bilayer show similar variations to the  $S_{CD}$  values of the *sn*-2 oleyl chain in POPC, as anticipated. The ordering of the palmitoyl chains in the bilayer achieved using is comparable and within the uncertainty of the available experimental data. Hence, KBFF best reproduces the ordering of lipid acyl chains. In theory a large bilayer is likely to reduce the influence of periodic boundary conditions and ameliorate convergence. This underlines the need to consider not only a wide range of properties but also the effect of sampling time and of system size when validating models. Hence the system with POPC bilayer with 512 lipid molecules was simulated. As shown by figure 3.3 the  $S_{cd}$  system has converged at lower values compared to that of the POPC lipid system with 128 lipids. Hence, it is apparent that system size and simulation time effects properties.

### 3.5 Conclusion

The simulations of phospholipids demonstrate that the KBFF lipid parameter set has good agreement with experimental values of phospholipids in the biologically relevant liquid crystalline phase with small deviations. Future work will be focused on studying the physical properties of pure lipid mixtures and developing parameters for cholesterol.

# Bibliography

- [1] Jacob D Durrant and J Andrew McCammon. Molecular dynamics simulations and drug discovery. *BMC biology*, 9(1):1–9, 2011. URL <https://doi.org/10.1186/1741-7007-9-71>.
- [2] Takefumi Yamashita. Toward rational antibody design: Recent advancements in molecular dynamics simulations. *International immunology*, 30(4):133–140, 2018. URL <https://doi.org/10.1093/intimm/dxx077>.
- [3] Benjamin Chantemargue. *In silico investigation of xenobiotic interactions with lipid bilayers and ABC membrane transporters, the case of ABCC4/MRP4*. PhD thesis, Université de Limoges; Univerzita Palackého (Olomouc, République Tchèque), 2018. URL <https://tel.archives-ouvertes.fr/tel-02418604/>.
- [4] Inna Ermilova. *Modeling of biomembranes: from computational toxicology to simulations of neurodegenerative diseases*. PhD thesis, Department of Materials and Environmental Chemistry, Stockholm University, 2019. URL <urn:nbn:se:su:diva-165940>.
- [5] Joachim Seelig and Anna Seelig. Lipid conformation in model membranes and biological membranes. *Quarterly reviews of biophysics*, 13(1):19–61, 1980. URL <https://doi.org/10.1017/s0033583500000305>.
- [6] Anna Seelig and Joachim Seelig. *Membrane Structure*. Academic Press, 2003. URL <https://doi.org/10.1016/B0-12-227410-5/00417-8>.
- [7] Derek Marsh. *Handbook of lipid bilayers*. CRC press, 2013. URL <https://doi.org/10.1201/b11712>.
- [8] Derek Marsh. Crc handbook of lipid bilayers. 1990. URL <https://doi.org/10.1201/b11712>.

- [9] Joachim Seelig and Nada Waespe-Sarcevic. Molecular order in cis and trans unsaturated phospholipid bilayers. *Biochemistry*, 17(16):3310–3315, 1978. URL <https://doi.org/10.1021/bi00609a021>.
- [10] Scott A Hollingsworth and Ron O Dror. Molecular dynamics simulation for all. *Neuron*, 99(6):1129–1143, 2018. URL <https://doi.org/10.1016/j.neuron.2018.08.011>.
- [11] Michael P Allen et al. Introduction to molecular dynamics simulation. *Computational soft matter: from synthetic polymers to proteins*, 23(1):1–28, 2004. URL <https://juser.fz-juelich.de/record/152581/files/FZJ-2014-02193.pdf>.
- [12] Wilfred F Van Gunsteren, Dirk Bakowies, Riccardo Baron, Indira Chandrasekhar, Markus Christen, Xavier Daura, Peter Gee, Daan P Geerke, Alice Glattli, Philippe H Hunenberger, et al. Biomolecular modeling: goals, problems, perspectives. *Angewandte Chemie International Edition*, 45(25):4064–4092, 2006. URL <https://doi.org/10.1002/anie.200502655>.
- [13] Wilfred F van Gunsteren and Jožica Dolenc. Biomolecular simulation: historical picture and future perspectives. *Biochemical Society Transactions*, 36:11–15, 2008. URL <https://doi.org/10.1042/BST0360011>.
- [14] Wilfred F van Gunsteren, Jožica Dolenc, and Alan E Mark. Molecular simulation as an aid to experimentalists. *Current opinion in structural biology*, 18(2):149–153, 2008. URL <https://doi.org/10.1016/j.sbi.2007.12.007>.
- [15] Martin Karplus and Gregory A Petsko. Molecular dynamics simulations in biology. *Nature*, 347(6294):631–639, 1990. URL <https://doi.org/10.1038/347631a0>.
- [16] Ya-Pu Zhao, Feng-Chao Wang, and Mei Chi. Molecular dynamics simulation and molecular orbital method. In *Handbook of Adhesion Technology*.
- [17] Nikos L Doltsinis. Molecular dynamics beyond the born-oppenheimer approximation: mixed quantum-classical approaches. *Computational nanoscience: Do it yourself*,

- pages 389–409, 2006. URL <https://juser.fz-juelich.de/record/51139/files/NIC-Band-31.pdf>.
- [18] Maricarmen Hernández-Rodríguez, Martha C Rosales-Hernández, Jessica E Mendieta-Wejebe, Marlet Martínez-Archundia, and Jose Correa Basurto. Current tools and methods in molecular dynamics (md) simulations for drug design. *Current medicinal chemistry*, 23(34):3909–3924, 2016. URL <https://doi.org/10.2174/0929867323666160530144742>.
- [19] Martin Karplus and J Andrew McCammon. Molecular dynamics simulations of biomolecules. *Nature structural biology*, 9(9):646–652, 2002. URL <https://doi.org/10.1038/nsb0902-646>.
- [20] Allen M P and Tildesley D J. *Computer Simulations of Liquids*, volume 2. Oxford University press, 1987. URL <https://oxford.universitypressscholarship.com/view/10.1093/oso/9780198803195.001.0001/oso-9780198803195>.
- [21] Loup Verlet. Computer” experiments” on classical fluids. i. thermodynamical properties of lennard-jones molecules. *Physical review*, 159(1):98, 1967. URL <https://doi.org/10.1103/PhysRev.159.98>.
- [22] Sidney Yip. *Handbook of materials modeling*. Springer Science and Business Media, 2007. URL <https://books.google.com/books?id=0sJaJ5juL9EC>.
- [23] Andrew R Leach. *Molecular Modelling*. Pearson, 2001. URL <https://www.pearson.com/us/higher-education/program/Leach-Molecular-Modelling-Principles-and-Applications-2nd-Edition/PGM251961.html?tab=order>.
- [24] Alexander D MacKerell Jr. Empirical force fields for biological macromolecules: overview and issues. *Journal of computational chemistry*, 25(13):1584–1604, 2004. URL <https://doi.org/10.1002/jcc.20082>.

- [25] Elizabeth A Ploetz, Sadish Karunaweera, Nikolaos Benteitis, Feng Chen, Shu Dai, Moon B Gee, Yuanfang Jiao, Myungshim Kang, Nilusha L Kariyawasam, Nawavi Naleem, et al. Kirkwood–buff-derived force field for peptides and proteins: Philosophy and development of kbff20. *Journal of Chemical Theory and Computation*, 17(5): 2964–2990, 2021. URL <https://doi.org/10.1021/acs.jctc.1c00076>.
- [26] Thorben Fröhlking, Mattia Bernetti, Nicola Calonaci, and Giovanni Bussi. Toward empirical force fields that match experimental observables. *The Journal of chemical physics*, 152(23):230902, 2020. URL <https://doi.org/10.1063/5.0011346>.
- [27] Soumil Y Joshi and Sanket A Deshmukh. A review of advancements in coarse-grained molecular dynamics simulations. *Molecular Simulation*, 47(10-11):786–803, 2021. URL <https://doi.org/10.1080/08927022.2020.1828583>.
- [28] Alexander P Lyubartsev and Alexander L Rabinovich. Force field development for lipid membrane simulations. *Biochimica et Biophysica Acta (BBA)-Biomembranes*, 1858(10): 2483–2497, 2016. URL <https://doi.org/10.1016/j.bbamem.2015.12.033>.
- [29] Jin Zhang, Haiyang Zhang, Tao Wu, Qi Wang, and David van der Spoel. Comparison of implicit and explicit solvent models for the calculation of solvation free energy in organic solvents. *Journal of chemical theory and computation*, 13(3):1034–1043, 2017. URL <https://doi.org/10.1021/acs.jctc.7b00169>.
- [30] Marketa Paloncyova, Karel Berka, and Michal Otyepka. Convergence of free energy profile of coumarin in lipid bilayer. *Journal of chemical theory and computation*, 8(4): 1200–1211, 2012. URL <https://doi.org/10.1021/ct2009208>.
- [31] PA Janmey and Paavo KJ Kinnunen. Biophysical properties of lipids and dynamic membranes. *Trends in cell biology*, 16(10):538–546, 2006.
- [32] Berta Gumí-Audenis, Luca Costa, Francesco Carlá, Fabio Comin, Fausto Sanz, and Marina I Giannotti. Structure and nanomechanics of model membranes by atomic force

- microscopy and spectroscopy: insights into the role of cholesterol and sphingolipids. *Membranes*, 6(4):58, 2016. URL <https://doi.org/10.3390/membranes6040058>.
- [33] Grzegorz Chwastek and Petra Schwille. A monolayer assay tailored to investigate lipid–protein systems. *ChemPhysChem*, 14(9):1877–1881, 2013.
- [34] M Gudmand, Matthias Fidorra, T Bjørnholm, and T Heimburg. Diffusion and partitioning of fluorescent lipid probes in phospholipid monolayers. *Biophysical journal*, 96(11):4598–4609, 2009.
- [35] Aleksander Czogalla, Michał Grzybek, Walis Jones, and Ünal Coskun. Validity and applicability of membrane model systems for studying interactions of peripheral membrane proteins with lipids. *Biochimica et Biophysica Acta (BBA)-Molecular and Cell Biology of Lipids*, 1841(8):1049–1059, 2014. URL <https://doi.org/10.1016/j.bbalip.2013.12.012>.
- [36] Reid C Van Lehn and Alfredo Alexander-Katz. Membrane-embedded nanoparticles induce lipid rearrangements similar to those exhibited by biological membrane proteins. *The Journal of Physical Chemistry B*, 118(44):12586–12598, 2014. URL <https://doi.org/10.1021/jp506239p>.
- [37] Harvey T McMahon and Jennifer L Gallop. Membrane curvature and mechanisms of dynamic cell membrane remodelling. *Nature*, 438(7068):590–596, 2005. URL <https://doi.org/10.1038/nature04396>.
- [38] RG Snyder, HL Strauss, and CA Elliger. Carbon-hydrogen stretching modes and the structure of n-alkyl chains. 1. long, disordered chains. *The Journal of Physical Chemistry*, 86(26):5145–5150, 1982.
- [39] David Poger and Alan E Mark. On the validation of molecular dynamics simulations of saturated and cis-monounsaturated phosphatidylcholine lipid bilayers: a comparison with experiment. *Journal of Chemical Theory and Computation*, 6(1):325–336, 2010. URL <https://doi.org/10.1021/ct900487a>.

- [40] Pouyan Khakbaz and Jeffery B Klauda. Investigation of phase transitions of saturated phosphocholine lipid bilayers via molecular dynamics simulations. *Biochimica et Biophysica Acta (BBA)-Biomembranes*, 1860(8):1489–1501, 2018. URL <https://doi.org/10.1016/j.bbamem.2018.04.014>.
- [41] David Poger, Wilfred F Van Gunsteren, and Alan E Mark. A new force field for simulating phosphatidylcholine bilayers. *Journal of computational chemistry*, 31(6):1117–1125, 2010. URL <https://doi.org/10.1002/jcc.21396>.
- [42] Susan L Duncan and Ronald G Larson. Comparing experimental and simulated pressure-area isotherms for dppc. *Biophysical journal*, 94(8):2965–2986, 2008. URL <https://doi.org/10.1529/biophysj.107.114215>.
- [43] Pouyan Khakbaz, Viviana Monje-Galvan, Xiaohong Zhuang, and Jeffery B Klauda. Modeling lipid membranes. *Biogenesis of Fatty Acids, Lipids and Membranes, Handbook of Hydrocarbon and Lipid Microbiology*, pages 1–19, 2017. URL [https://doi.org/10.1007/978-3-319-50430-8\\_52](https://doi.org/10.1007/978-3-319-50430-8_52).
- [44] Scott E Feller. Molecular dynamics simulations of lipid bilayers. *Current opinion in colloid & interface science*, 5(3-4):217–223, 2000. URL [https://doi.org/10.1016/S1359-0294\(00\)00058-3](https://doi.org/10.1016/S1359-0294(00)00058-3).
- [45] Eleni Alexandri, Raheel Ahmed, Hina Siddiqui, Muhammad I Choudhary, Constantinos G Tsiafoulis, and Ioannis P Gerothanassis. High resolution nmr spectroscopy as a structural and analytical tool for unsaturated lipids in solution. *Molecules*, 22(10):1663, 2017.
- [46] Norbert Kučerka, John F Nagle, Jonathan N Sachs, Scott E Feller, Jeremy Pencer, Andrew Jackson, and John Katsaras. Lipid bilayer structure determined by the simultaneous analysis of neutron and x-ray scattering data. *Biophysical journal*, 95(5):2356–2367, 2008.

- [47] Radek Macháň and Martin Hof. Lipid diffusion in planar membranes investigated by fluorescence correlation spectroscopy. *Biochimica et Biophysica Acta (BBA)-Biomembranes*, 1798(7):1377–1391, 2010.
- [48] Michael P Allen and Mark R Wilson. Computer simulation of liquid crystals. *Journal of computer-aided molecular design*, 3(4):335–353, 1989.
- [49] Jeffery B Klauda, Richard M Venable, J Alfredo Freites, Joseph W OConnor, Douglas J Tobias, Carlos Mondragon-Ramirez, Igor Vorobyov, Alexander D MacKerell Jr, and Richard W Pastor. Update of the charmm all-atom additive force field for lipids: validation on six lipid types. *The journal of physical chemistry B*, 114(23):7830–7843, 2010.
- [50] RW Pastor and AD MacKerell Jr. Development of the charmm force field for lipids. *The journal of physical chemistry letters*, 2(13):1526–1532, 2011. URL <https://doi.org/10.1021/jz200167q>.
- [51] Oliver Berger, Olle Edholm, and Fritz Jähnig. Molecular dynamics simulations of a fluid bilayer of dipalmitoylphosphatidylcholine at full hydration, constant pressure, and constant temperature. *Biophysical journal*, 72(5):2002–2013, 1997.
- [52] Callum J Dickson, Lula Rosso, Robin M Betz, Ross C Walker, and Ian R Gould. Gafflipid: a general amber force field for the accurate molecular dynamics simulation of phospholipid. *Soft Matter*, 8(37):9617–9627, 2012.
- [53] Gayani Nadeera Pallewela. *Theory and simulation of liquids and liquid mixtures*. Kansas State University, 2016. URL <https://krex.k-state.edu/dspace/handle/2097/32495>.
- [54] Nilusha Lakmali Kariyawasam Manachchige. *Computer simulations of small molecules and proteins in solution*. PhD thesis, 2019. URL <https://krex.k-state.edu/dspace/handle/2097/40214>.

- [55] Mohomed Nawavi Mohomed Naleem. *Molecular dynamics simulations of aqueous ion solutions*. PhD thesis, 2017. URL <https://krex.k-state.edu/dspace/handle/2097/35458>.
- [56] John G Kirkwood and Frank P Buff. The statistical mechanical theory of solutions. i. *The Journal of chemical physics*, 19(6):774–777, 1951.
- [57] Weria Pezeshkian, Himanshu Khandelia, and Derek Marsh. Lipid configurations from molecular dynamics simulations. *Biophysical journal*, 114(8):1895–1907, 2018.
- [58] Alan J Robinson, W Graham Richards, Pamela J Thomas, and Michael M Hann. Head group and chain behavior in biological membranes: a molecular dynamics computer simulation. *Biophysical journal*, 67(6):2345–2354, 1994.
- [59] Derek Marsh and Tibor Páli. Lipid conformation in crystalline bilayers and in crystals of transmembrane proteins. *Chemistry and physics of lipids*, 141(1-2):48–65, 2006.
- [60] Derek Marsh and Tibor Páli. The protein–lipid interface: perspectives from magnetic resonance and crystal structures. *Biochimica et Biophysica Acta (BBA)-Biomembranes*, 1666(1-2):118–141, 2004.
- [61] David A Mannock, Ruthven NAH Lewis, Todd PW McMullen, and Ronald N McElhaney. The effect of variations in phospholipid and sterol structure on the nature of lipid–sterol interactions in lipid bilayer model membranes. *Chemistry and physics of lipids*, 163(6):403–448, 2010.
- [62] Alexandru Botan, Fernando Favela-Rosales, Patrick FJ Fuchs, Matti Javanainen, Matej Kanduc, Waldemar Kulig, Antti Lamberg, Claire Loison, Alexander Lyubartsev, Markus S Miettinen, et al. Toward atomistic resolution structure of phosphatidylcholine headgroup and glycerol backbone at different ambient conditions. *The Journal of Physical Chemistry B*, 119(49):15075–15088, 2015.
- [63] H Hauser, I Pascher, and S Sundell. Preferred conformation and dynamics of the glycerol

- backbone in phospholipids. an nmr and x-ray single-crystal analysis. *Biochemistry*, 27(26):9166–9174, 1988.
- [64] Derek Marsh. Lipid-binding proteins: structure of the phospholipid ligands. *Protein science*, 12(9):2109–2117, 2003.
- [65] Scott E Feller and Alexander D MacKerell. An improved empirical potential energy function for molecular simulations of phospholipids. *The Journal of Physical Chemistry B*, 104(31):7510–7515, 2000.
- [66] Berk Hess, Carsten Kutzner, David Van Der Spoel, and Erik Lindahl. Gromacs 4: algorithms for highly efficient, load-balanced, and scalable molecular simulation. *Journal of chemical theory and computation*, 4(3):435–447, 2008.
- [67] Herman JC Berendsen, JPM van Postma, Wilfred F Van Gunsteren, ARHJ DiNola, and Jan R Haak. Molecular dynamics with coupling to an external bath. *The Journal of chemical physics*, 81(8):3684–3690, 1984.
- [68] Berk Hess, Henk Bekker, Herman JC Berendsen, and Johannes GEM Fraaije. Lincs: a linear constraint solver for molecular simulations. *Journal of computational chemistry*, 18(12):1463–1472, 1997.
- [69] Pekka Mark and Lennart Nilsson. Structure and dynamics of the tip3p, spc, and spc/e water models at 298 k. *The Journal of Physical Chemistry A*, 105(43):9954–9960, 2001.
- [70] HJC Berendsen, JR Grigera, and TP Straatsma. The missing term in effective pair potentials. *Journal of Physical Chemistry*, 91(24):6269–6271, 1987.
- [71] Herman JC Berendsen, James PM Postma, Wilfred F van Gunsteren, and Jan Hermans. Interaction models for water in relation to protein hydration. In *Intermolecular forces*, pages 331–342. Springer, 1981.
- [72] William L Jorgensen, Jayaraman Chandrasekhar, Jeffrey D Madura, Roger W Impey,

- and Michael L Klein. Comparison of simple potential functions for simulating liquid water. *The Journal of chemical physics*, 79(2):926–935, 1983.
- [73] Ulrich Essmann, Lalith Perera, Max L Berkowitz, Tom Darden, Hsing Lee, and Lee G Pedersen. A smooth particle mesh ewald method. *The Journal of chemical physics*, 103(19):8577–8593, 1995.
- [74] D Peter Tieleman, Siewert-Jan Marrink, and Herman JC Berendsen. A computer perspective of membranes: molecular dynamics studies of lipid bilayer systems. *Biochimica et Biophysica Acta (BBA)-Reviews on Biomembranes*, 1331(3):235–270, 1997. URL [https://doi.org/10.1016/s0304-4157\(97\)00008-7](https://doi.org/10.1016/s0304-4157(97)00008-7).
- [75] Siewert J Marrink, Alex H De Vries, and D Peter Tieleman. Lipids on the move: simulations of membrane pores, domains, stalks and curves. *Biochimica et Biophysica Acta (BBA)-Biomembranes*, 1788(1):149–168, 2009. URL [https://doi.org/10.1016/S0006-3495\(01\)75894-8](https://doi.org/10.1016/S0006-3495(01)75894-8).
- [76] Alex H de Vries, Indira Chandrasekhar, Wilfred F van Gunsteren, and Philippe H Hünenberger. Molecular dynamics simulations of phospholipid bilayers: Influence of artificial periodicity, system size, and simulation time. *The Journal of Physical Chemistry B*, 109(23):11643–11652, 2005. URL <https://doi.org/10.1021/jp0507952>.
- [77] Christofer Hofsäß, Erik Lindahl, and Olle Edholm. Molecular dynamics simulations of phospholipid bilayers with cholesterol. *Biophysical journal*, 84(4):2192–2206, 2003. URL [https://doi.org/10.1016/S0006-3495\(03\)75025-5](https://doi.org/10.1016/S0006-3495(03)75025-5).
- [78] Michael Patra, Mikko Karttunen, Marja T Hyvönen, Emma Falck, Peter Lindqvist, and Ilpo Vattulainen. Molecular dynamics simulations of lipid bilayers: major artifacts due to truncating electrostatic interactions. *Biophysical journal*, 84(6):3636–3645, 2003. URL [https://doi.org/10.1016/S0006-3495\(03\)75094-2](https://doi.org/10.1016/S0006-3495(03)75094-2).
- [79] Mark James Abraham, Teemu Murtola, Roland Schulz, Szilárd Páll, Jeremy C Smith, Berk Hess, and Erik Lindahl. Gromacs: High performance molecular simulations

- through multi-level parallelism from laptops to supercomputers. *SoftwareX*, 1:19–25, 2015. URL <https://doi.org/10.1016/j.softx.2015.06.001>.
- [80] Michael Patra, Mikko Karttunen, Marja T Hyvönen, Emma Falck, and Ilpo Vattulainen. Lipid bilayers driven to a wrong lane in molecular dynamics simulations by subtle changes in long-range electrostatic interactions. *The Journal of Physical Chemistry B*, 108(14):4485–4494, 2004. URL <https://doi.org/10.1021/jp031281a>.
- [81] Qaiser Waheed. *Molecular Dynamic Simulations of Biological Membranes*. PhD thesis, KTH Royal Institute of Technology, 2012. URL <https://www.diva-portal.org/smash/record.jsf?pid=diva2%3A551948&dswid=9264>.
- [82] Kechuan Tu, Douglas J Tobias, and Michael L Klein. Constant pressure and temperature molecular dynamics simulation of a fully hydrated liquid crystal phase dipalmitoylphosphatidylcholine bilayer. *Biophysical journal*, 69(6):2558–2562, 1995. URL [https://doi.org/10.1016/S0006-3495\(95\)80126-8](https://doi.org/10.1016/S0006-3495(95)80126-8).